Title
Assessing the potential for luminescence dating in the Mojave Desert, California

Author
Roder, Belinda J.

Publication Date
2012

Peer reviewed|Thesis/dissertation

UNIVERSITY OF CALIFORNIA
Los Angeles

Assessing the potential for luminescence dating in the Mojave Desert, California

A thesis submitted in partial satisfaction
of the requirements for the degree Master of Science
in Geology

by

Belinda Joan Roder

2012

ABSTRACT OF THE THESIS

Assessing the potential for luminescence dating

in the Mojave Desert, California

by

Belinda Joan Roder

Master of Science in Geology

University of California, Los Angeles, 2012

Professor Edward J. Rhodes, Chair

A reliable, widely applicable geochronological tool is an imperative part of neotectonic studies. While there are several geochronological techniques available for Quaternary research, each method has its limitations. Luminescence dating has huge potential for these kinds of studies, as it relies on commonly occurring minerals (namely quartz and K-feldspar), directly dates the event of interest, can be applied over a wide range of timescales, and gives ages without any complex calibration required.

While optically stimulated luminescence (OSL) dating of quartz and infrared stimulated luminescence (IRSL) dating of K-feldspar work well in many regions, these techniques have proven problematic for many OSL users and dating specialists in

southern California. Issues of low sensitivity and low (dim) signal intensity often yield inconsistent and questionable results. It is the aim of this study to develop an improved methodology for luminescence dating in this region.

From the El Paso Peaks trench site on the central Garlock fault, several samples were collected for luminescence dating. Conventional quartz OSL protocols did not yield accurate age estimates. Various K-feldspar IRSL protocols were tested in this study, while new techniques were developed and assessed. Experimentation with two novel procedures, the selective SAR48-12 and SACoR approaches, demonstrate great potential for innovative new ways to deal with problematic samples. The novel K-feldspar isothermal thermoluminescence (ITL) approach gives encouraging results, although further research is warranted to determine how robust and widely applicable the technique is. Because of the pervasive problem of incomplete bleaching in the region, single-grain K-feldspar IRSL measurements may be the best technique for isolating well bleached grains and determining precise and accurate age estimates.

The thesis of Belinda Joan Roder is approved.

Raymond V. Ingersoll

An Yin

Edward J. Rhodes, Chair

University of California, Los Angeles

2012

Contents

List of Tables

List of Figures

Acknowledgements

I would like to graciously thank the UCLA Department of Earth and Space Sciences, the Southern California Earthquake Center (award #11198), and the Los Angeles Basin Geological Society for their generous funding and support of this project. I am especially thankful for my advisor, Dr. Edward J. Rhodes, for giving me the opportunity to obtain this advanced degree and grow as a scientist. His patience while teaching me and immersing me in a new field was invaluable. Our collaboration has enabled me to present my research at a number of professional conferences, as well as publish a manuscript in a well-known scientific journal. His support and encouragement has given me the confidence to begin my career as a geologist, with the passion and drive to continue learning and growing.

I would also like to thank my family and friends for their encouragement and support during my graduate program. I will always remember the camaraderie and friendships that evolved in office 5631, and throughout the ESS department.

1. Introduction

Geochronology is an essential part of neotectonic studies and seismic-hazard assessments. Without reliable geochronological data, fundamental questions, such as the degree to which fault loading and strain release are constant, cannot be answered. Moreover, in a situation where GPS data are not available, determining the geochronology of offset features is the only way to determine fault slip rates. While there are several geochronological techniques available on the timescale of the Quaternary Period, each method has its limitations (Figure 1). Many of these techniques require the presence of a specific, often scarce, material that has to occur in the appropriate context, such as organic remains for radiocarbon dating (Lian and Roberts, 2006). Furthermore, many of these dating methods are only applicable over short timescales, and the calculated age may not directly date the event of interest. A more advantageous dating method would be one that can be applied to ubiquitous materials, directly dates the event of interest, can be applied to a wide age range, and gives ages without any complex calibration required (Lian and Roberts, 2006).

The nature of geomorphic features from which slip rates can be determined for neotectonic studies and seismic hazard assessments can be difficult to date reliably. Faulted landforms, such as offset alluvial fans or terrace risers, are well preserved in desert regions, but organic matter for radiocarbon dating is generally absent or sparse. Detrital charcoal has been found in fine-grained playa deposits in semi-arid regions (Dawson et al., 2003), but is less commonly preserved in alluvial-fan deposits where offset landforms necessary for measuring rates of strike-slip movement are often found.

Uranium-series dating of carbonate cements can provide a minimum age for sediment deposition, but this is constrained by the availability of appropriate material (Fletcher et al., 2010), which is rare. Terrestrial cosmogenic nuclide (TCN) dating of alluvial-fan features in arid regions may be problematic and associated with large uncertainties (van der Woerd et al., 2006; Behr et al., 2010). Furthermore, truncation of sediment profiles by erosion or incremental deposition of overlying deposits will both cause problems for this technique. Optically stimulated luminescence (OSL) and infrared stimulated luminescence (IRSL) dating has huge potential in desert regions, as they rely on the occurrence of quartz and feldspar grains, which are ubiquitous in this kind of environment.

In regions where quartz and feldspar grains have favorable luminescence characteristics, the resolution (±5 to 10% at 1σ) and age range (1 to ~200,000 years) of OSL make it an appropriate geochronological tool for neotectonic investigations (Rhodes, 2011). Good agreement has been shown between OSL ages and independent methods, indicating the effectiveness of this technique (Figure 2). The quartz single-aliquot regenerative-dose (SAR) protocol (discussed in section 2.2.1) is a highly robust method capable of dealing with issues such as incomplete bleaching in sediment with sensitive quartz, while still yielding precise and accurate age estimate (Rhodes et al., 2010). However, while standard quartz OSL procedures work well in many regions, this method has proven problematic in southern California for many OSL users and dating specialists (e.g. Lawson et al., in press; Mahan, S., pers. comm., 2011; Owen, L.A., per. comm., 2011; Rendell et al., 1994; Rittenour, T., pers. comm., 2011). Quartz from this

region displays generally low sensitivity and low (dim) signal intensity, often yielding inconsistent results (Figure 3). It is the goal of this project to contrive improved methods for the OSL and IRSL dating of quartz and feldspar in southern California, as well as develop the isothermal thermoluminescence (ITL) method for feldspar, in an effort to establish an improved geochronological tool for this region. The aim is to make the first steps toward determining reliable age estimates on the timescales of 10 to 10,000 years, with uncertainties in the range of ±5 to 10% or better.

1.1 Project Objectives

The goal of this project is to assess existing methods, and to explore and refine new approaches to luminescence dating in the Mojave Desert region. To do so, the El Paso Peaks (EPP) site along the central Garlock fault was revisited (Figure 4). At this site, paleoseismic trench studies have resulted in an extensive radiocarbon chronology composed of 35 samples and constraining six well resolved earthquake events (McGill and Rockwell, 1998; Dawson et al., 2003). For this study, the EPP trench was re-opened and samples were collected for luminescence dating, bracketed by units already dated in previous studies. This allows for the assessment and optimization of our luminescence dating procedures by comparison with the existing radiocarbon chronology. A pilot study was first conducted at the Christmas Canyon West site (Figure 4), located 30 km to the east of EPP, in an effort to assess the luminescence characteristics of quartz and feldspar in this region.

While quartz from this region is expected to have low sensitivity, IRSL dating of feldspar may prove to be much more useful. Various feldspar IRSL protocols are used in this study, while new techniques are developed and assessed. This study employs the first use of the isothermal thermoluminescence (ITL) signal for age determinations of feldspar. It is also the first systematic study of feldspar IRSL age results relative to radiocarbon control ages for neotectonic applications. Through various measurement protocols and subsequent observations, theoretical and practical methods have been developed in an effort to determine an improved approach for dating feldspar in this region.

2. Introduction to luminescence dating

Optically stimulated luminescence (OSL) dating was introduced in 1985 (Huntley et al.) as a method to determine the time elapsed since sediments were last exposed to sunlight. The method is based on the luminescence signal emitted by commonly occurring minerals, primarily quartz and K-feldspar. The amount of luminescence emitted by the sample during laboratory measurement can be used as a proxy for the amount of energy it received during burial. When divided by the amount of radiation it receives per year, known as the dose rate, the age of the deposit (time elapsed since the sample was last exposed to sunlight) can be calculated.

The term optically stimulated luminescence includes the luminescence stimulated by photons of any wavelength, including infrared stimulated luminescence (IRSL) and blue and/or green stimulated luminescence (Aitken, 1998). Another form of luminescence dating is that stimulated by heat, called thermoluminescence (TL). Here, luminescence will be used as a general term, and it will be specified when referring to quartz OSL, feldspar IRSL, or thermoluminescence (TL). Below, I provide an introduction to this dating technique; a more detailed review of the general concept of luminescence dating can be found in Aitken (1998), Duller (2008), and Rhodes (2011).

2.1 Physical basis of luminescence dating

Minerals, such as quartz and feldspar, contain various types of (point) defects within their crystal lattices, and at these locations, electrons may become trapped. There are many types of defects, including those formed by elemental substitution

(Rhodes, 2011) (e.g. Ti replacing Si in quartz) or by a negative-ion vacancy, whose negative charge deficiency will attract and trap free electrons (Aitken, 1998). When these minerals are deposited and buried, they are subjected to low levels of environmental ionizing radiation coming from the decay of radioactive elements such as uranium, thorium (as well as their daughter isotopes) and potassium-40 in the surrounding sediment, as well as by cosmic rays and, to a lesser extent, rubidium-87 (Aitken, 1998). This flux of radiation provides energy that causes electrons within atoms in the crystal lattice to become excited from their valence positions into the conduction band (Figure 5). A very small proportion of the electrons may become trapped at defects within the forbidden energy gap between the valence band and the conduction band, and is referred to as trapped charge (Aitken 1998; Duller, 2008). The effectiveness for luminescence dating of a given trap type is dictated by its depth below the conduction band, E, which determines how stable the electron will be and, therefore, how long electrons may stay trapped. With time, more electrons accumulate in traps and the trapped charge population grows.

Upon exposure to sunlight or heating (typically between 200°C to 400°C), electrons are evicted from their traps and diffuse through the crystal until either another type of trap or a recombination center is found. Some recombination centers, known as luminescence centers, cause the electron to loose the energy they gained during irradiation, and a portion of that energy may be emitted in the form of a photon. In the simplest case, the light emitted by the sample is a product of the amount of trapped charge, and hence the amount of accumulated energy that has been absorbed

due to the flux of ionizing radiation (Aitken, 1998). The bleaching by sunlight reduces the trapped charge population to a low level, effectively "zeroing" the sample.

To illustrate how this process can be used for dating, an analogy of a rechargeable battery as a mineral grain can be useful (Figure 6; Rhodes, 2011). When a mineral grain is exposed to sunlight during transportation, trapped electrons are released, similar to a battery being depleted of its charge. After deposition and burial, the mineral is again exposed to environmental radiation, causing trapped charge to accumulate, analogous to recharging a battery. After the sediment is collected, the sample is stimulated by light in the laboratory and the minerals release their stored energy in the form of light, again, much like depleting a battery. The brightness of the luminescence emitted from the sample is proportional to the amount of energy that the sample received while it was buried. Laboratory measurements are used to calculate the amount of laboratory radiation that is equivalent to the amount of radiation (measured in grays (Gy), which represents 1 joule of energy, in the form of ionizing radiation, per kilogram of matter) received in nature, known as the equivalent dose (D_e). When combined with the dose rate, or rate at which the sample received radiation through time, the luminescence age of the sample can be derived using Equation [1] (Aitken, 1998):

$$\textbf{age (years)} = \frac{\textbf{equivalent dose } (\mathbf{D_e})(\mathbf{Gy})}{\textbf{dose rate } \left(\frac{\mathbf{Gy}}{\mathbf{year}}\right)}$$

2.2 Laboratory measurement of OSL

In the laboratory, optical stimulation is used to release the electrons stored within minerals and the observed signal is termed optically stimulated luminescence (OSL). As soon as the light is switched on, the minerals begin luminescing; as the measurement continues, the trapped charge is emptied and the signal decreases (Figure 7). For quartz, the signal initially decays very rapidly, and then at a slower rate. The initial rapid decay is due to luminescence originating from traps that are easiest to bleach, and is known as the "fast" component (Bailey et al., 1997). The luminescence emitted by traps that are not as easily bleach are the "medium" and "slow" components. Bright, sensitive quartz is dominated by the fast component, whereas dim quartz is dominated by the medium and slow components (Figure 3). Feldspars, however, display slower initial decay (Figure 7), and because of this difference in the decay form, the shape of the decay curve can be used to check the purity of quartz separated from feldspar for luminescence measurements.

The light used to stimulate the minerals needs to be of a significantly different wavelength to that of the luminescence emission of the mineral. Quartz OSL has a peak emission of 365 to 380 nm (i.e. near-ultraviolet), and thus blue-green LEDs (light emitting diodes) with an emission centered around 470 nm are a good choice of light source (Aitken, 1998; Duller, 2008; Rhodes, 2011). The stimulation source is required to have a narrow range of wavelengths (stimulation window) so that the photomultiplier tube, used to measure the luminescence signal, does not detect this light. The photomultiplier tube contains a glass filter used to prevent light from the stimulation

source from being detected, but designed to allow UV light to pass through the detection window. When stimulating with blue-green LEDs, a common filter to use is the Hoya-U340, whichblocks wavelengths greater than 380 nm (Figure 8) (Duller, 2004).

Another method of stimulation is to use LEDs that emit in the infrared (800-900 nm) (Aitken, 1998). The luminescence signal emitted from this kind of stimulation, termed infrared stimulated luminescence (IRSL), is most commonly observed from feldspars. Quartz does not emit an IRSL signal at room temperature, and this fact can be used to check the purity of quartz fractions used for OSL measurements.

2.2.1 Single-aliquot regenerative dose (SAR) procedure

The single-aliquot regenerative dose (SAR) procedure, first described by Murray and Wintle (2000a; 2003), is now widely used as a method for determining the equivalent dose (D_e). The SAR procedure is composed of a series of cycles (Table 1). In the first cycle, the luminescence signal (signified as L) due to the radiation that the sample was exposed to in nature (L_N) is measured. In the second cycle, the sample is given an artificial dose of radiation in the laboratory and the OSL signal is then measured, which is the first laboratory regenerated signal, L_1. Each subsequent cycle gives a different regenerative dose (20 Gy, 40 Gy, 60 Gy, etc.) followed by an OSL signal measurement (L_2, L_3, L_4, etc). Each measurement is preceded by a preheat, such as heating the sample to 220°C for 10 s at 10°C s^{-1}, to remove any unstable charge.

The luminescence sensitivity, or luminescence efficiency per unit trapped charge, of an aliquot (small portion of a sample mounted on an aluminum disc) has been

observed to change over the course of a SAR measurement sequence. Therefore, it is necessary to monitor sensitivity change for each OSL measurement. The SAR procedure measures the sensitivity change of quartz by giving a fixed dose, known as the test dose, in the second half of each cycle followed by measurement of the luminescence signal (T_N, T_1, T_2, etc.). Any sensitivity change is recognized by plotting the ratio of each natural and regenerative-dose measurement to the following sensitivity measurement (L_x/T_x), known as a growth curve, or dose-response curve. The D_e is calculated by the intercept of the natural luminescence signal with the regenerated curve (Figure 9).

The SAR protocol includes several tests that can be used to determine the behavior of each aliquot (Wintle and Murray, 2006). The recycling test is comprised of a repeat measurement of one of the radiation doses (Figure 9: point L_7/T_7). If the protocol is appropriate and able to correct for changes in sensitivity, then the ratio between the two sensitivity-corrected luminescence signals, known as the recycling ratio, should be one. In practice, a ratio between 0.9 and 1.1 is considered acceptable (Duller, 2008). A ratio greater or less than this implies that the protocol or the samples are not appropriate.

A dose recovery test involves bleaching an aliquot (by daylight or an artificial light source), irradiating the aliquot with a known dose (i.e. 10 Gy), and then applying a SAR procedure to see if the measured dose matches the given dose. If the SAR procedure recovers the given dose, then it can be considered appropriate. However, if a sample fails a dose recovery test, it is unlikely that the D_e calculated for that sample is correct (Duller, 2008).

2.2.2 Feldspar IRSL

Feldspar is measured in a similar manner to quartz, using a SAR protocol, but is stimulated with IR diodes (800-900 nm). The use of feldspar minerals for luminescence dating can be, in some cases, more useful than quartz for several reasons. It emits a significantly brighter luminescence signal than quartz, which is of particular interest to this project, as the quartz from the study area is known to be dim. Feldspar also has a much higher level of luminescence saturation and, therefore, has a higher upper age limit than quartz (ca. 500 ka). However, feldspar suffers from a number of effects that make the determination of precise age estimates challenging. Feldspar bleach more slowly than quartz, making incomplete bleaching a common problem. Feldspar also have an internal dose rate contribution arising from potassium, which must be accounted for when calculating the dose rate. The main effect that feldspar suffers from is termed anomalous fading.

2.2.2.1 Anomalous fading

Anomalous fading is the phenomenon displayed by feldspar, where after irradiation, the intensity of the luminescence signal decreases as the sample is stored in the laboratory (Wintle, 1973). It is termed anomalous because the physical parameters of the traps, namely trap depth, suggest that it should be stable. While the nature of anomalous fading is not well understood, it is thought to arise from quantum-mechanical tunneling of trapped charge from their stable traps to nearby recombination centers (Aitken, 1998). It has been shown that most feldspar species suffer from

anomalous fading (Spooner, 1994), and that it is common among sediment samples from North America (Huntley and Lamothe, 2001).

Because anomalous fading of feldspar leads to an age underestimation, storage tests must be undertaken to determine the fading rate, or g value (Aitken, 1998). The g value corresponds to the percentage fading loss per decade of time, and can be used to correct IRSL ages for fading samples (Huntley and Lamothe, 2001). The g value can be calculated from Equation [2] (Huntley and Lamothe, 2001):

$$I = I_c \left[1 - \frac{g}{100} \log_{10}\left(\frac{t}{t_c}\right)\right]$$

where I is the IRSL intensity measured at time t after irradiation, and I_c is the intensity when $t = t_c$ (the latter being the time of the prompt measurement). Storage tests consist of irradiation of a sample followed by a prompt measurement of the IRSL (I). The sample is then given the same irradiation, stored in the laboratory and measured again at a later time (I_c).

3. Site Descriptions

The goal of this project is to assess the luminescence characteristics of quartz and feldspar in the Mojave Desert region, and determine an enhanced procedure for luminescence dating. To do so, two sites along the central Garlock fault were explored. The Christmas Canyon West site was chosen as a pilot study to examine the luminescence characteristics of alluvial-fan sediments in this kind of desert environment. The El Paso Peaks site was the primary target of this study, from which samples were collected for luminescence dating from a trench with an existing radiocarbon chronology in an effort to assess the performance of quartz OSL and K-feldspar IRSL. In this section, the site details and sampling methods will be described.

3.1 El Paso Peaks

The El Paso Peaks (EPP) paleoseismic site (N35°26’39.1”, W117°40’53.5”) is located along the central Garlock fault, approximately 2.3 km west of where the fault crosses Highway 395 (Figure 4). The site is situated near the eastern end of the 3.5km-wide releasing bend in the Garlock fault that is responsible for the Koehn Lake pull-apart basin (McGill and Rockwell, 1998). At this site, paleoseismic trench investigations have been performed by McGill and Rockwell (1998) and Dawson et al. (2003). In this study, a trench from the previous study was re-opened to collect a series of samples for OSL dating.

3.1.1 Geomorphology

At the EPP site, the Garlock fault strikes between N63° and 67°E (Dawson et al., 2003). The trench site is located on a small playa that is bounded to the north by the El Paso Mountains and to the south by a shutter ridge composed of deeply dissected, older alluvial-fan gravels that has been translated along the fault (Figure 10). The playa is blocked from freely draining by a small Holocene alluvial fan to the northeast. The ephemeral stream that has formed the alluvial fan is also the primary source of sand and silt that comprise the playa sediments.

McGill and Rockwell (1998) note that two major fault strands are geomorphically expressed at this site. Immediately west of the trench site, the fault is expressed as a single primary trace. To the east, the fault splays into two main traces. These two traces parallel each other for about 1.7 km. Farther east, the southern strand dies out, where the northern strand bends slightly southward and continues. McGill and Rockwell (1998) suggested that the northern strand is the active strand at this location, as indicated by clear evidence for strike-slip faulting in the form of offset, deflected and abandoned stream channels. Adjacent to the site, a large drainage channel that is deeply incised into old alluvial-fan deposits has been sinistrally offset 200-250 m; an abandoned channel to the east has been offset an even greater distance. The southern strand lacks any evidence for offset or deflected streams, suggesting subdued activity.

3.1.2 Sedimentology

The playa sediments at the EPP trench site are composed primarily of sand and silt. McGill and Rockwell (1998) noted that near the northern and eastern boundaries of the playa, the uppermost playa deposits interfinger with, and grade into, Holocene alluvial-fan gravels, while at the southern boundary of the playa, the sediments interfinger with colluvial gravels derived from the shutter ridge. The trench in this study is located near the center of the playa, well enough away from the playa boundaries that there were no significant gravel deposits present, except in the uppermost layers.

The playa sediments consist of beds that range from approximately 1 cm to 25 cm in thickness (Figure 11). The majority of the beds grade from sand into silt, and are thought to represent individual flood events or pulses of a single flood event (Dawson et al., 2003). McGill and Rockwell (1998) note that the sandy portions are thicker and more coarse near the northeastern edge of the playa, closer to the source, and that the proportion of sand increases upsection, possibly as the result of the progradation of the alluvial fan into the basin, causing the source to move progressively closer. McGill and Rockwell (1998) suggested that the playa formed by damming due to progradation of the alluvial fan to the northeast, which has blocked the site from freely draining.

The exceptional stratigraphy at the EPP site, composed of distinctive units of graded sand and silt, make this a prime location for geochronological investigations. The units, previously identified and named by McGill and Rockwell (1998) and Dawson et al.

(2003), are distinctive, usually laterally continuous, and relatively easy to correlate across the length of the trench.

3.1.3 Field methods

The EPP trench was re-excavated in May 2009 to approximately 5 m deep and 20 m long (Figure 12). The backfill from the previous trench was recognizable during excavation because it was very loose sediment. Because the majority of the sediment here was so loose, it was necessary for the trench to be wide with many benches, to prevent the trench walls from collapsing. The trench was re-excavated to approximately the location of the previous trench studies on its east side, as recognized by finding the former sampling grid and several sample location flags still intact from Dawson's excavations in 2000 (Dawson et al., 2003) (Figure 13). Samples were collected from the east wall of the trench because the stratigraphy was intact and easily recognizable there. After the trench was excavated, the east wall was cleaned to remove any smeared sediment or gouge created by the backhoe, and to clearly expose the stratigraphy. Sally McGill from California State University, San Bernadino, co-investigator on this project and present at both previous trench studies at EPP, identified the stratigraphic units from the previous studies.

3.2.3.1 Sampling

Units that are constrained by pre-existing radiocarbon dates were targeted for OSL dating. Samples were collected primarily from sandy units to obtain sufficient material of the target grain sizes (spanning 125-250 μm). Very thin units were avoided in

an attempt to sample units wide enough that the sample tubes (mostly 6 cm diameter, some 3 cm diameter) stayed within one unit, which presumably represents one depositional event, although this is not necessarily the case. Because of the rapid, episodic deposition characteristic of the floods likely responsible for these sediments, the interval of time being sampled probably represents a few hours, or possibly up to a week for the finer sediments.

Samples were collected from metal tubes (mostly 10 cm long, 6 cm diameter; some samples were collected in smaller tubes), which were pushed into a cleaned vertical face of the section. Sample tubes were sealed at each end and taken back to the lab for preparation and measurement. Dose rates were determined for each sample location based on in-situ gamma spectrometery, using a calibrated EG&G microNomad portable NaI gamma spectrometer, measured for around 20 minutes at each sample location (Table 2). The water content of the sediment used in age calculations was based on present water content measured using small additional sediment samples.

3.2 Christmas Canyon West

The Christmas Canyon West (CCW) site (N35°31’10.5”, W117°23’15.8”) was recognized as a location to obtain slip rates on this portion of the Garlock fault (Figure 4). This broad, gently sloping alluvial-fan surface has been moderately dissected by fluvial processes, resulting in a series of bars and channels. LIDAR (Light Detection and Ranging) images of the area show clear evidence for fault movement in the form of offset alluvial fan features (Figure 14). A test pit, approximately 1 m deep, was dug

within a bar that has clearly been truncated by fault movement (Figure 15). The sediment is dominated by coarse sand, with lesser amounts of fine- to medium-gravel (Rhodes, E.J., pers. comm., 2011). The sediment is not well-stratified, which may be an indicator of bioturbation. Five samples were collected for luminescence dating, paying careful attention to avoid any roots or burrows that may introduce younger grains into older layers. The dose rate for each sample was measured using the same procedure as at EPP, as described in the previous section.

4. Laboratory methods

4.1 Sample preparation

Luminescence sediment samples were prepared in the laboratory under controlled lighting using amber and red safelights, whose wavelength will not evict any significant trapped charge within the mineral grains. Sample tubes were opened, and the outer 1-2 cm of each end removed due to possible light exposure during sample collection. The ends of each sample were reserved for subsequent beta dose rate determination using ICP-MS and ICP-OES; these data have been measured for CCW but not yet for EPP. The water content was measured for each sample location to be included in dose rate calculations. Water in the sediment will absorb radiation, thereby attenuating the dose rate and, if ignored, may cause an age underestimation or overestimation (Aitken, 1985).

The bulk, or central part, of each sediment sample was wet sieved to extract a range of grain sizes (>400 µm, 250-400 µm, 175-250 µm, 125-175 µm, 100-125 µm, <100 µm), with the modal grain size chosen for analysis. Samples were treated with dilute HCl to remove carbonates. K-feldspar grains were separated out of the sample using 2.58 g/cm^3 lithium metatungstate (LMT). Quartz grains were treated with 40% concentrated hydrofluoric acid (HF) for 100 minutes to remove the outer alpha irradiated layer of the grains and dissolve any remaining feldspars (mainly plagioclase), and then sieved to remove any partially dissolved mineral fragments that formed during HF treatment.

Quartz grains were then separated from the remaining heavy minerals using 2.70 g/cm^3 LMT. The quartz fraction is sieved a second time to remove any mineral fragments, which were broken apart during the HF treatment.

For conventional multiple-grain single aliquot measurements, grains were mounted in a single layer on aluminum discs using silicone oil. Medium-sized aliquots, 2 mm in diameter (~100 grains) were generally used. Small aliquots (≤1 mm) were tested to see if bright grains could be isolated, and large aliquots (>2 mm) were used to see if a large signal could be attained. Neither size resulted in significant advantage, and therefore, medium aliquots were used throughout the study.

4.2 Luminescence measurement parameters

Luminescence measurements were made using TL-DA-20 Risø automated reader. The majority of measurements were made within the Department of Earth and Space Sciences at the University of California, Los Angeles, with early several measurements of CCW samples made at the Institute for Integrated Research in Materials, Environments, and Society (IIRMES) at California State University, Long Beach (CSULB).

4.2.1 Quartz

The single-aliquot regenerative-dose (SAR) protocol, described in section 2.2.1, is now the most widely used method for OSL dating of quartz (Murray and Wintle, 2000a;

2003). A typical SAR protocol was applied to quartz grains from EPP and CCW (Table 3). Samples were measured in the UV region using a standard Hoya U340 filter.

Table 3 shows a conventional SAR sequence used to measure quartz OSL in this study. Typically, 12 aliquots (small portions of a sample mounted on aluminum discs) were measured for each sample. After measurement of the natural luminescence signal (L_N), regenerative doses are administered, followed by a preheat to remove any unstable charge. Aliquots were first stimulated with IR diodes to check for feldspar contamination, and then were stimulated with blue LEDS to measure the luminescence signal (L_1). Next, a uniform test dose of 1.15 Gy (10 s of irradiation) was given, followed by a second preheat. After IR stimulation, the luminescence signal was again measured (T_1). The cycle was completed with a "hot bleach" OSL treatment at 220°C to help remove any remaining charge that could contribute to subsequent age determinations (Wallinga et al., 2007).

4.2.2 Feldspar

IRSL dating of K-feldspar can be advantageous in regions where quartz displays low sensitivity and dim signals because feldspar generally has high OSL and IRSL sensitivity, resulting in a relatively bright signal. This may lead to better precision in age estimates and a lower chance of signal contamination. Feldspar also has a higher saturating dose, that is, a higher level of charge can be trapped before all of the electron traps are full and the sample is "saturated". The higher level of saturation causes the feldspar growth curve to be able to date older sediments. However, feldspar suffers

from anomalous fading and has a slower bleaching rate than quartz, both of which can make the dating of feldspar challenging.

Various feldspar IRSL protocols were tested in this study. Initial measurements of K-feldspar from CCW were measured using a conventional IRSL dating protocol comprised of stimulation for 40 s at 60°C, following a preheat of 260°C for 10 s.

An essential component of feldspar IRSL dating is the measurement of an anomalous fading rate (g value; Aitken, 1985), which is used to correct the apparent feldspar ages. Recent work has been focused on identifying a feldspar signal that is less prone to fading, or does not fade at all. A lower fading rate requires a smaller correction to be made. Thomsen et al. (2008) have shown that the laboratory fading rate is dependent on the stimulation and detection window, and have identified the post-IR elevated temperature IR signal (the IRSL signal measured at 225°C after an initial IR stimulation at 50°C) as having the lowest fading rate. This is the signal arising from an elevated temperature IRSL measurement after an initial, lower temperature IRSL measurement, when using a blue detection window such as the BG3+BG39 (~360-480 nm) filter combination. This post-IR elevated temperature IRSL protocol was employed in this study in an attempt to target the more stable feldspar signals and minimize fading.

Buylaert et al. (2009) demonstrated that the post-IR IRSL measurement protocol can be used to measure the equivalent dose (D_e) and fading rate, resulting in a smaller correction factor than that measured at low stimulation temperatures. This study employs the same post-IR IR SAR measurement protocol as Buylaert et al. (2009) for

feldspar IRSL measurements of samples from El Paso Peaks and Christmas Canyon West (Table 4). To achieve the blue detection window required for this protocol, the filters in the photomultiplier tube were changed from Hoya U340 (340 nm) to a BG3+BG39 combination (~360-480 nm). After the regenerative dose is administered, the aliquot is preheated to 250°C and held there for 60 s to remove any unstable charge. The aliquot is then stimulated with IR diodes at 50°C for 100 s, followed by a second IR stimulation at 225°C for 100 s. The SAR cycle is completed after a test dose is administered and the same preheat and IR stimulations are repeated. At the end of each SAR cycle, a "hot bleach" is administered at 290°C for 40 s to reduce any remaining charge that might contribute to the subsequent IR_{50} or IR_{225} signals, and reduce recuperation.

The post-IR IRSL measurement protocol allows for three separate signals to be observed from each feldspar aliquot. The initial preheat (250°C held for 60 s) allows the ITL signal to be measured (see section 4.2.2.2). The first IR stimulation at 50°C, which is referred to here as the IR_{50} signal, is similar to conventional low temperature IRSL measurements and is useful for age determinations. The subsequent IR stimulation at 225°C, the post-IR IR signal (referred to as the IR_{225} signal), is the main signal of interest in the original Buylaert et al. (2009) protocol, as it was shown to have a lower fading rates and therefore requires the smallest age correction (Thomsen et al., 2008).

4.2.2.1 Fading rates

Because of the ubiquity of the anomalous fading of feldspar, g values were calculated for selected feldspar samples from EPP. At the end of the regular IRSL

measurement cycle (the prompt measurement, I_c), the samples were given an irradiation (i.e. for 40 s). The samples were then stored in the laboratory and re-measured at a later date (the faded measurement, I). This is referred to here as the "long" method for fading tests. Using Equation 2, g values were calculated for each signal (ITL, IR_{50}, IR_{225}) from each sample. The precision of the g value can be improved with an increasing number of delayed measurements (Auclair et al., 2003). However, because of time limitations, this study used one delayed measurement.

The "quick fade" method was developed in this study as a rapid method to obtain g values from a number of short delayed measurements. This protocol gives aliquots a dose (i.e. 100 s irradiation) and then measures the signal after five different delay times (i.e. 410 s, 1320 s, etc.). By plotting IRSL intensities versus the log of time elapsed since irradiation, a g value can be deduced from the slope of the line connecting the points (Auclair et al., 2003) (Figure 16).

4.2.2.2 Isothermal thermoluminescence (ITL)

Another signal that can be observed from the post-IR IRSL protocol for feldspar is the isothermal thermoluminescence (ITL) signal. This signal is observed during the preheat treatment (Table 4), and involves heating the sample to 250°C and holding it there for 60 s (Figure 17). The resulting TL curve is treated as though it were an OSL or IRSL decay curve by using a wide window close to the start of the isothermal portion of the treatment, subtracting a background signal based on the end of the isothermal treatment, and correcting for sensitivity changes using a SAR protocol. This method has

been applied to quartz in an attempt to extend the luminescence age range (Murray and Wintle, 2000b; Choi et al., 2006; Huot et al., 2006), but there is no record of its application to feldspar in the literature.

4.2.2.3 Single-grain luminescence measurements

Measurement of the luminescence signal emitted by individual sand-sized grains can be done using a focused laser. Using a single-grain reader that attaches to the Risø automated reader, 100 individual grains of a sample, contained within individual 0.3 mm by 0.3 mm holes in an aluminium disc, can be measured using a standard SAR protocol. Studies have demonstrated that, for quartz, up to 95% of the luminescence measured comes from less than 5% of the grains (Duller, 2008). Therefore, during single-grain measurements, most grains do not emit sufficient luminescence to yield D_e determinations. The main disadvantage of using single-grain measurements is the time and effort required in obtaining useful data, especially for dim samples. However, single-grain analysis is a useful tool for targeting only the grains that emit a bright luminescence signal within a sample that is generally dim. For this reason, single-grain IRSL was used to measure three K-feldspar samples from EPP.

5. Results

Results presented in this chapter are first organized by sampling site, and then broken down by luminescence measurement method. Age estimations from both CCW and EPP are presented, with some key observations highlighted. A summary of luminescence dating results can be found in Table 5.

5.1 El Paso Peaks luminescence results

At this site, 11 samples were dated in this study using luminescence dating. Four different luminescence dating methods were investigated in an attempt to enhance conventional procedures, as well as develop new ones. Within some of the methods, different measurement protocols were explored, and the differences between them are explained in Chapter 4. The performance of the different luminescence methods will be assessed by comparing the age results with the well-established radiocarbon chronology of Dawson et al. (2003) (Table 6).

5.1.1 EPP Quartz OSL age results

Quartz from samples J0140 through J0145 was dated using conventional OSL (blue-green stimulation) using the SAR protocol of Murray and Wintle (2000a; 2003); age results are shown in Table 5. Aliquots from each sample displayed consistently dim OSL signals (~20-60 counts/0.16s), as a result of low luminescence sensitivity (Figure 18a). In contrast, a bright quartz sample will emit an initial OSL of ~30,000 counts/0.16 s

(Figure 3). The decay curves generated during luminescence measurement show a relatively high contribution from the slowly decaying components (a limiting factor for precise age estimations), but display little sensitivity increase during the SAR cycle (a positive feature indicating suitability of the SAR protocol in correcting for sensitivity changes). Equivalent dose (D_e) values of aliquots from the same sample are highly scattered, with a wide range of variation, suggestive of a mixture of completely and incompletely bleached grains (Figure 19). Because of this variation, the lowest consistent D_e values were used for age estimations because they are most likely to be completely bleached and free of any residual signal that would result in an age overestimation. Recycling is good (between 0.9 and 1.1) within their 1σ errors, suggesting that the SAR protocol is appropriate for correcting for sensitivity changes.

Quartz OSL age estimations from EPP are not in stratigraphic order and are, therefore, not internally consistent (Figure 20). These ages are highly underestimated when compared to the radiocarbon ages from adjacent stratigraphic units. Sample J0142, collected at 102 cm depth, gives a D_e of -0.18, resulting in an age of -70±50 years old (i.e. 70 years in the future, but with a large uncertainty), while the radiocarbon ages indicate it should be approximately 600-700 years old. Samples J0144 and J0145, collected from depths of 143 and 168 cm, respectively, give ages close to 0 years. Clearly, these samples do not only suffer from incomplete bleaching, but some other effect that causes low D_e values and age underestimations.

A dose recovery experiment was conducted on sample J0145 to test the appropriateness of the SAR protocol and evaluate the samples ability to store doses. 12

aliquots were given a 5.7 Gy dose, and this dose was recovered immediately using a SAR protocol. A value of 5.4±0.2 Gy was recovered, indicating that these aliquots are able to store doses on short timescales. This experiment was repeated with a 10-day delay between irradiation and measurement. This time, 6.2±0.3 Gy (1.08±0.04 times the given dose) was recovered, implying that the OSL signal from these samples do not fade in a manner similar to feldspar, resulting in age underestimations. To investigate whether the quartz grains are extremely sensitive to the laboratory safe lights, the same quartz aliquots were given the same 5.7 Gy dose and then exposed to an amber (590 nm) LED safelight at 18.5 cm distance for one hour. A value of 5.6±0.3 Gy (0.97±0.05 times given dose) was recovered, indicating that exposure to the laboratory safelights is not causing low D_e values observed for the natural signal. Quartz from this site seems to suffer from some unknown effect that prevents determination of the correct natural dose values.

5.1.2 EPP Feldspar IRSL age results

Feldspar IRSL age estimates at EPP were obtained using the relatively new post-IR IRSL protocol (Buylaert et al., 2009; Table 4). Using this protocol, three different signals can be observed: ITL, IR_{50}, and IR_{225}. A summary of the feldspar ITL and IRSL age estimates for samples J0137 through J0149 from EPP can be found in Table 5.

The feldspar IRSL age estimates at EPP are variable, with highly scattered D_e values for aliquots of a single sample. Because this high variation is likely caused by incomplete bleaching, the lowest consistent D_e values were used for age estimations. Recycling is good for all three signals and sensitivity change is low, with most samples

displaying either no significant change or a slight decrease in sensitivity during the course of the SAR cycle. Some thermal transfer (signals generated by heating, resulting in charge relocation from other traps; Rhodes, 2011) was observed for IR_{50} and IR_{225} signals in the form of a non-zero signal observed during the zero dose SAR measurement. The IR_{50} age estimates are in agreement with, or slightly lower than, the IR_{225} age estimates (Table 5), which suggests that the IR_{225} signal is less bleachable, or bleaches at a slower rate than the IR_{50} signal, and may be more prone to anomalous fading.

5.1.2.1 ITL, selective SAR48-12 and SACoR results

The ITL signals measured from feldspar appear to provide preliminary age estimates consistent with ^{14}C ages, although uncorrected for fading. The ITL age estimates for the uppermost three samples, J0137, J0138, and J0139, are 1580±110, 1770±130 and 1490±110 years old, respectively. The age estimations are highly overestimated, probably as a result of incomplete bleaching. The preliminary age estimations for the lower eight samples, before fading corrections, are internally consistent, in stratigraphic order, and compatible with the ^{14}C ages. It should be noted that samples J0143 and J0144 were collected from the same thick, sandy horizon (unit 118). It is unclear whether this unit was deposited by multiple events over an extended period of time, or whether the ITL age for J0144 is an overestimate.

A new method, referred to as the selective SAR48-12 protocol, was tested in this study. This protocol measures the natural SAR cycle for 48 aliquots of one sample. The

L_n/T_n (the sensitivity-corrected natural IRSL signal intensity) values are then analyzed in order to identify the 12 aliquots that give the lowest values, which are assumed to be the most well-bleached. These aliquots are used for the rest of the SAR cycle and D_e determination. This method aims at identifying and measuring only the most well-bleached and consistent aliquots, resulting in a more precise age estimate and decreased machine time. The selective SAR48-12 protocol was tested on sample J0140 (Table 7). The IR_{50} signal gave a group of consistent D_e values around 1 Gy (Figure 21). The relatively low variation of D_e values for all 12 aliquots demonstrates the method's main purpose of targeting aliquots with low D_e, which are presumably the most well bleached. The IR_{225} signal gives D_e values that are more highly scattered, but does result in a group of sensible results around 1.5 Gy.

The single-aliquot combined regenerative (SACoR) protocol was developed and explored in this study as a method to reduce the impact of fading and obtain a larger number (48) of L_n/T_n results. This protocol measures the natural SAR cycle for 48 discs. Then, groups of 6 discs receive different regenerative doses (0, 10, 20, 40, 80, 120, 160, 200 s of irradiation). This data are combined and fitted with a single multiple-aliquot growth curve to provide 48 D_e values. This method allows the discs to be stored after the doses are administered, and this means that the effects of anomalous fading can be reduced. In this case, a delay of 35 days between irradiation and IRSL measurement was employed, reducing potential fading effects by two decades (i.e. the g value times two) in comparison to a regular SAR protocol. The SACoR method was tested on sample J0143 (Figure 22). The IR_{50} signal gave a group of sensible results around 2.5 Gy,

consistent with stratigraphically neighboring ^{14}C ages. While several discs gave the same D_e value for IR_{50} and IR_{225}, the IR_{225} signal gave only one value compatible with the 2.5 Gy from the IR_{50} signal. Most discs from the IR_{225} signal gave values around 8 Gy, which represents a significant overestimation and is probably a result of the slower bleaching rate of the IR_{225} signal, as well as incomplete bleaching at the time of deposition.

5.1.2.2 Fading

Fading rates, or g values, were obtained from two different methods for feldspar samples from EPP. The "long method" for fading tests, in which the initial IRSL measurement was compared to the IRSL intensity after the samples had been irradiated and stored for some length of time, gave a range of g values. Table 8 shows the average g values for 12 aliquots of each sample. ITL gives an average g value of 3% decade. The IR_{50} signal gives a slightly higher average g value of 4% per decade. The IR_{225} signal gives g values close to 0, with sample J0149 giving a value of 17% per decade, which is higher than expected. Variations in g values between aliquots of the same sample may represent different fading properties of different feldspar species, different fading properties of grains with different histories, and intrinsic uncertainties in the ratio.

Fading rates obtained using the quick fade method are summarized in Table 8. Aliquots are given a dose and then a full SAR cycle measured (including sensitivity correction), and the whole procedure repeated for 5 different short delay times (e.g. 100 s, 300 s, etc.). On a plot of luminescence intensity (I) versus the log of time elapsed since irradiation, the g value can be obtained from the slope of the line connecting these

points (Figure 16; Auclair et al., 2003). Table 9a shows g values for 2 aliquots of each sample, obtained using a protocol that administers the preheat (which is the ITL measurement) after the pause that allows for fading. There appears to be a wide range of variation in g values between aliquots of the same sample, as well as between the different signals observed. Table 9b shows g values obtained using a similar protocol, except with the preheat administered before the pause (therefore, no ITL data is measured here). Again, there is wide scatter between g values for each signal of the same sample, as well as variation between aliquots of the same sample.

5.1.2.3 Single-grain IRSL

Single-grain IRSL measurements were made for samples J0140, J0143 and J0145 (Table 10). This method, just like the single-aliquot method, resulted in a wide scatter of D_e values for each signal from all three samples. However, taking the lowest group of D_e values gives sensible results. Single-grain IR_{50} and IR_{225} age estimates are in good agreement for both J0140 and J0145, as well as consistent with radiocarbon ages. Single-grain age estimates for J0143 seem to be slightly underestimated when compared to the radiocarbon ages. Although very time consuming relative to the single-aliquot method, the single-grain method may be the best choice for identifying relatively bright grains that will yield accurate D_e determinations, despite the issue of incomplete bleaching. At this stage, no directly measured fading data are available for single grain determinations, and it is unclear what impact these data might have on these encouraging preliminary age estimates.

5.1.2.4 SEM analysis

Select samples from EPP were analyzed under the Scanning Electron Microscrope (SEM) using the LEO 1430 VP system and electron-dispersive X-ray (EDX) spectroscopy at UCLA in an attempt to identify the minerals present. The quartz fraction from sample J0145 was examined to check the effectiveness of the mineral separation technique. While the fraction appeared to be comprised mostly of quartz, some feldspar grains (and possibly other minerals) were present (Figure 23).

K-feldspar fractions from J0140 and J0149 were analyzed to determine which feldspar species were present. Approximately 10 grains were analyzed, and while not all were feldspar species, Andesine, Bytownite and Oligoclase were identified. However, chemical composition of the surface of many grains indicated high iron content (3-30 molar percent) (Figure 24). This iron present of the surface of the grains may contribute to the relatively dim signals displayed by feldspar. In response to this, these feldspar fractions were subjected to a quick hydrofluoric acid (HF) treatment (~10 min, diluted concentration of ~10%) in an attempt to etch off the iron coating. Un-etched samples that had single-grain IRSL measurements initially giving only ~18% of grains emitting a useful IRSL signal, now gave ~50% of grains with a useful IRSL signal after the quick HF etch. This suggests that the iron present on the surface of the grains does indeed diminish the luminescence signal emitted by feldspar at this site. However, comparison of IRSL age estimates for three samples before and after the HF treatment show no systematic improvement (Table 11).

5.2 Christmas Canyon West luminescence results

Five samples were collected from Christmas Canyon West (CCW) as a pilot study to assess the luminescence characteristics of both quartz and feldspar in this region of the Mojave Desert. There is no independent age control available at this site to compare with the luminescence age estimates. While it is hoped that future studies may to be undertaken at this site to determine fault slip rates on this portion of the Garlock fault, these results should be considered preliminary.

5.2.1 CCW Quartz OSL age results

Quartz samples from CCW are consistently dim, and show high contributions from the slowly decaying components, rendering conventional SAR protocols unsuccessful at yielding accurate age estimates (Figure 25a). To overcome this issue, the "synthetic super-aliquot" approach was explored, developed by Ed Rhodes and introduced in Bristow et al. (2010) as a method for dating Antarctic dune samples that also displayed extremely low OSL sensitivity. This method discards signals from distinctly outlying high dose values (results beyond 3 sigma from the mean of the remaining doses), which are considered to suffer from partial bleaching (Figure 26). The signals from the remaining consistent aliquots are summed at each dose point and at each sensitivity correction measurement point, and are fitted with a single growth curve. This method is used to overcome the issue of low counts that are a product of low signal sensitivity. Preliminary quartz OSL age estimates that were calculated using this

approach appear internally consistent (Figure 27). While the uppermost three samples agree with initial feldspar IRSL age estimates (measured at 60°C) for the same samples, although uncorrected for fading, the lower two samples are highly underestimated when compared to the subsequent feldspar IRSL age estimates (Table 5).

5.2.2 CCW Feldspar IRSL age results

Feldspar samples from CCW are relatively dim, producing a low number of counts (Figure 25b). Initial feldspar measurements were made using a conventional IRSL protocol comprised of stimulation for 40 s at 60°C, following a preheat of 260°C for 10 s. The resulting age estimations, although not corrected for fading, appear in agreement with quartz synthetic super-aliquot OSL results from the same samples, and are also internally consistent. Later measurements were made using the post-IR IRSL protocol (Table 4), which resulted in generally older ages (Table 5).

6. Discussion

In this chapter, the results of this study and their implications are discussed. This discussion is based on the purpose of this study, which is to determine what does and does not work for luminescence dating in the Mojave Desert region.

6.1 EPP quartz OSL

6.1.1 Sample characteristics

Quartz grains from both the CCW and EPP sites are consistently dim (low luminescence intensity). These characteristics have been noted in other tectonically active areas (i.e. New Zealand, Peru, etc.), and have been attributed to the young sedimentary history of the grains (e.g. Preusser et al., 2006; Steffen et al., 2009; Rhodes, 2011). Pietsch et al. (2008) noted that the sensitivity of quartz increases linearly with distance downstream from the source, and ascribe this to repeated cycles of irradiation and bleaching. Laboratory experiments have demonstrated that, for initially non-luminescent grains, repeated cycles of irradiation and bleaching can cause the grains to become "switched on", resulting in increased luminescence sensitivity (Pietsch et al., 2008). In tectonically active areas, such as the Mojave Desert, where quartz (and feldspar) grains have been relatively recently eroded out of bedrock, they may not have had the opportunity for numerous cycles of deposition (irradiation) and erosion (bleaching). Consequently, the luminescence sensitivity of the grains is low. In contrast, quartz from Australia is particularly suited for OSL dating, and is characterized by high

luminescence intensity and sensitivity (Rhodes et al., 2007; Pietsch et al., 2008; Fitzsimmons et al., 2010), which has been attributed to the numerous cycles of irradiation, bleaching and heating experienced by the quartz grains during their sedimentary history (Pietsch et al., 2008).

6.1.2 Luminescence characteristics

The decay curves for nearly all quartz OSL measurements from both sites show a lack of the fast component, and are mostly dominated by the medium and slow components. This makes those samples more susceptible to feldspar contamination, which was observed in the SEM analysis of quartz fractions from EPP samples. Quartz OSL age estimates at EPP are generally underestimated when compared to the radiocarbon ages, as well as the feldspar IRSL ages (Table 5, Figure 20). Steffen et al. (2009) explored samples from Peru that have poor quartz OSL characteristics and result in age underestimations, and have determined that this is due to the fast component not being the dominant signal, along with a medium component that is thermally unstable. A possible solution to circumvent the thermally unstable medium component is to isolate the fast component using a modified SAR protocol, which will presumably result in a more accurate age estimate (Steffen et al., 2009). While it is beyond the scope of this study, future work could be aimed at testing this method in an effort to deal with the poor quartz luminescence characteristics in southern California and obtain accurate age estimates. However, this method is unlikely to make a significant improvement for samples such as those from EPP and CCW, which are extremely dim.

6.1.3 Equivalent dose variation

The high variation in equivalent doses (D_e) for different aliquots of the same sample measured by quartz OSL at both sites indicates a variety of dose values of the individual grains. This may be due to post-depositional grain mixing (i.e. bioturbation), potential variations in the dose rate, or partial bleaching at the time of deposition (Duller, 2008). Examination of the stratigraphy during sampling showed no clear evidence of significant grain mixing, such as burrows or roots. However, bioturbation cannot be ruled out as responsible for some grain mixing. While no determinations of dose rate heterogeneity have been made at this stage, it is possible that some variation in D_e values observed may come from this source, though it is unlikely that these would be as large as the observed D_e variation. This variation may also be due to some inherent problem of the SAR method, for reasons not yet known. However, the principle cause of variability in D_e values is thought to come from partial bleaching. This is consistent with the samples having been recently eroded out of bedrock causing the low OSL sensitivity and relatively slow bleaching (due to large quantities of charge in less bleachable traps) (Rhodes, 2011).

6.1.4 Quartz OSL age estimates

Because of the evidence for incomplete bleaching at the time of deposition, the approach of choosing the lowest, consistent D_e values for age determination seems sensible. However, this method has resulted in clear age underestimations at EPP

relative to the radiocarbon control ages (Table 5, Figure 20). The presence of negative ages (J0142) and ages of nearly zero (J0144 and J0145) suggest that there is something complex going on with quartz grains at this site. Dose recovery tests indicate that the OSL signals from these samples do not fade in a manner similar to feldspar, resulting in D_e underestimations. Experiments also indicate that the quartz is not extremely sensitive to laboratory safelights, so accidental bleaching during sample preparation is not the cause of age underestimations. There is some other effect responsible for the prevention of accurate quartz OSL age estimations in this region, although the cause has not been identified unambiguously. While recycling ratios indicate that the SAR protocol is not inappropriate for these samples, future work should test a variety of protocols to try and overcome issues of low sensitivity and highly variable D_e values. The possibility of signal contamination by other minerals, either as grains within the quartz separates, or as inclusions within the quartz grains themselves, can be explored further.

6.2 EPP feldspar IRSL

6.2.1 Sample characteristics

Like the quartz grains, feldspar grains from both sites are generally dim and have low sensitivity. Dim IRSL signals have been observed by other luminescence users in the Mojave Desert, and seems to be typical of this region (Mahan, per. comm.; Rendell et al., 1994; Rittenour, pers. comm.). The issue of dim signals may be mitigated by making larger discs (i.e. >200 grains), which would allow more bright grains to contribute to signal and D_e estimation. The dim IRSL signals may also be attributed, at least in part, to

the iron observed on the surface of EPP feldspar grains by SEM analysis. IRSL intensities were significantly brighter after a quick (~10 min) etch in diluted HF.

6.2.2 Feldspar IRSL age results

The post-IR IRSL protocol tested in this study appears to be an appropriate SAR protocol, as indicated by good recycling ratios and little sensitivity change. Because of evidence for partial bleaching in the form of highly variable D_e values between aliquots of the same sample, choosing the lowest group of consistent D_e values appears to be a sensible method for age estimations. However, a range of age estimates is observed from the three signals involved in the protocol: ITL, IR_{50}, and IR_{225}. While the radiocarbon ages of Dawson et al. (2003) do not constrain the luminescence samples as tightly as one would hope, they do provide a range of ages with which the luminescence dates can be compared to. The upper three samples from EPP, J0137, J0138 and J0139, give age overestimates for all three signals, particularly for ITL. This may suggest that the ITL signal bleaches more slowly than the IR_{50} and IR_{225} signals. This would probably be expected, as this approach does not specifically target charge in light-sensitive electron traps. These three samples come from layers deposited under higher energy conditions than lower samples (Figure 12). This probably represents a lateral migration of the alluvial fan out into the playa basin, and deposition within this period is probably dominated by short distance transport under conditions of higher flow, probably corresponding to periods of intense precipitation.

The lower samples do not seem to suffer from such extreme incomplete bleaching, and so perhaps the upper three samples experienced an extremely rapid, high-energy depositional event or were deposited at night. In general, the novel ITL feldspar approach provides preliminary raw (fading uncorrected) age estimates in good agreement with the radiocarbon ages for the lower eight samples (Figure 28). The raw IR_{50} and IR_{225} age estimates for these samples are more erratic and are generally overestimated, though a few samples give age underestimations.

The selective SAR48-12 method appears to be a viable method for identifying and isolating the most well bleached aliquots. By measuring the natural cycle for 48 aliquots, one can identify the 12 aliquots with the lowest D_e values on which to complete the SAR cycle and determine the D_e of the sample. This method is especially useful for samples, such as those from CCW and EPP, which show evidence of partial bleaching.

The SACoR method appears to a useful means of obtaining age estimations by measuring the natural signal of 48 discs and then giving groups of six discs different regenerative doses, which are then combined to create a growth curve. The main advantage of this method is to reduce the effects of fading, and further research is warranted to determine the optimum protocol for this method.

Single-grain IRSL measurements on samples J0140 and J0145 are extremely encouraging. Single-grain IR_{50} and IR_{225} age estimates are in good agreement for both samples J0140 and J0145, and these ages are consistent with the radiocarbon ages. These measurements appear to overcome the issue of age overestimation by isolating

the most well bleached grains for D_e determination. However, fading assessments are necessary for single-grain feldspar IRSL measurements, and future research should focus on the most efficient way to do this. Single-grain measurements may be the most useful technique for accurate age estimations on dim feldspar in the Mojave Desert region.

6.2.2.1 Fading

Fading rates, or g values, obtained using the "long" method, in which initial IRSL measurements are compared to measurements made after the sample has been store in the laboratory for some length of time, give a range of generally sensible results. Huntley and Lamothe (2001) sediment samples from North America gave g values than range from 2% to 10% per decade. The g values obtained using this method primarily fall within this range. Negative g values are likely the product of the luminescence increasing during the delayed measurement, and may be a product of thermal transfer, measurement artifacts, or simply reflect uncertainties in the g value.

Using the "quick fade" method, both with the preheat done before and after the delay, g values were significantly higher. It appears as though the loss to fading is rapid at first, and then levels out to a slower rate after some time. This may suggest that with longer delay times, the g values calculated would be significantly lower. At this stage, fading rates obtained using both methods are considered unreliable.

The ITL age estimates at EPP are in good agreement with radiocarbon ages before fading corrections are applied. This striking consistency seems unlikely to be a coincidence. Perhaps the ITL signal contains a residual dose that is proportional to the

amount of fading the sample experiences, effectively balancing out. Further research into the optimum way to measure and calculate fading rates is needed, in particular for ITL measurements.

6.3 Christmas Canyon West results

Because there is no independent age control available at the CCW site, we cannot be sure of the validity of our luminescence ages. Initial quartz OSL ages appear in agreement with IRSL age measured at 60°C. However, later measurements made using the post-IR IRSL measurement protocol are significantly older than the initial measurements. This suggests that, as is the case at EPP, the quartz OSL measurements result in age underestimates. However, the synthetic super-aliquot approach is still a good method for overcoming issues of dim signals and low intensity, even if its application is not useful owing to unreliable OSL signals .

7. Conclusions

The El Paso Peaks trench site provides us with an excellent opportunity to refine and assess new luminescence dating approaches by comparison with a robust independent chronological framework. This developmental study has resulted in abundant data, including 33 conventional multiple-grain single-aliquot regenerative dose (SAR) dating measurements, single-grain feldspar measurements, experimentation with two novel methods (the selective SAR48-12 and SACoR approaches), and the novel application of feldspar isothermal thermoluminescence (ITL) measurements. This study was aimed at overcoming the issues that impede luminescence dating in the Mojave Desert region, specifically dim luminescence intensity and low sensitivity. Although it is too early to say which approach is best, substantial progress has been made toward this goal. In particular, the single-grain IRSL approach and selective SAR48-12 are encouraging, and the excellent apparent agreement between preliminary ITL age estimates and ^{14}C age control demands further detailed investigation. In future work, these methods may be applied to other regions that experience similar problems, such as other parts of southern California, New Zealand, and high Asia.

7.1 Quartz OSL

At both the EPP and CCW sites, conventional quartz OSL SAR protocols are not able to yield accurate age estimates. Basing age calculations, for both quartz and feldspar, on the minimum equivalent dose (D_e) values appears to be a good method when incomplete bleaching is the dominant issue responsible for inter-aliquot variation.

At EPP, quartz OSL ages are consistently underestimated. This may be due to mineral inclusions within the quartz that are contributing to the signal, or some other complex phenomenon that has not yet been identified. Further research is needed to determine if quartz OSL measurements will be able to provide accurate age estimates, either with refined preparation procedures, or by modifying the luminescence measurement protocols.

7.2 Feldspar IRSL

Feldspar IRSL measurements at EPP are promising, and appear to have the potential to provide accurate age estimates. The novel feldspar ITL measurements are also encouraging; however, further validation is required to determine how sound and widely applicable this technique is. The IR_{50} and IR_{225} signals also appear to have the potential to produce accurate age estimates, but further experiments are required to determine the optimum approach. While fading rates are expected to be low, future research is required to determine the best method for measuring g values and applying them to correct feldspar IRSL ages.

Experimental procedures developed in this study demonstrate the great potential for innovative ways to deal with problematic samples. The SAR48-12 method appears to be a sound method for dealing with dim samples by measuring only the most wellbleached aliquots. The SACoR method was developed as a way to save machine time and reduce problems caused by fading.

Single-grain IRSL measurements may be the most advantageous way of obtaining accurate and precise age estimates in the Mojave Desert region. This method can overcome the issue of incomplete bleaching and isolate the relatively bright grains that will yield accurate age estimates. Further research into single-grain feldspar IRSL measurements at EPP is warranted to determine the most effective way of applying this dating method.

Table 1

Simplified SAR sequence

Step	Treatment	Measured
1	Give Dose, D_i	
2	Preheat[b] (160-300°C for 10 s)	
3	Stimulate[c] for 100 s at 125°C	L_i
4	Give test dose, D_t	
5	Heat[b] to 160°C	
6	Stimulate for 100 s at 125°C	T_i
7	Return to 1	

[a] For the natural cycle, $i = 0$ and $D_0 = 0$ Gy.

[b] Aliquot cooled to <60°C after heating. In step 1 and 5, the TL signal can be observed, but is not used in routine applications.

[c] Stimulation time is dependent on simulation light intensity.

[d] L_i and T_i are derived from the initial OSL signal (0.8 s) minus the background estimated from the last part of the stimulation curve (8 s).

Table 1. A simplified single aliquot regenerative-dose (SAR) protocol, modified from Murray and Wintle (2000a). This protocol is repeated as a series of cycles, and used to determine the equivalent dose (D_e) of a sample. In the first cycle, the natural luminescence signal due to radiation that the sample experienced in nature is measured. In each subsequent cycle, the sample is given an artificial dose of radiation (20 Gy, 40 Gy, 60 Gy, etc.), followed by an OSL measurement. These regenerative doses are used to define the dose response curve which, when compared to the natural luminescence signal, the D_e can be calculated.

Table 2. Dose rate data at El Paso Peaks

Quartz

Field code	Laboratory code	Stratigraphic unit	K (%)	Th (ppm)	U (ppm)	Gamma dose rate (mGy/a)		1 sigma uncertainty (mGy/a)	Total dose rate (mGy/a)		1 sigma uncertainty (mGy/a)
EPP11-04	J0140	100	1.42	5.91	1.83	1.018	±	0.003	2.57	±	0.10
EPP11-05	J0141	110	1.39	6.60	1.95	1.053	±	0.003	2.62	±	0.10
EPP11-06	J0142	114	1.36	7.09	2.25	1.114	±	0.003	2.69	±	0.10
EPP11-07	J0143	118	1.39	7.33	2.26	1.145	±	0.003	2.75	±	0.10
EPP11-08	J0144	118	1.36	7.38	2.30	1.143	±	0.003	2.73	±	0.10
EPP11-09	J0145	128b	1.35	6.86	2.19	1.093	±	0.003	2.64	±	0.10

Feldspar

Field code	Laboratory code	Stratigraphic unit	K (%)	Th (ppm)	U (ppm)	Gamma dose rate (mGy/a)		1 sigma uncertainty (mGy/a)	Total dose rate (mGy/a)		1 sigma uncertainty (mGy/a)
EPP11-01	J0137	90	1.401	5.929	1.875	1.038	±	0.003	3.16	±	0.173
EPP11-02	J0138	92	1.389	5.841	1.886	1.011	±	0.003	3.11	±	0.159
EPP11-03	J0139	98	1.363	5.962	1.880	1.007	±	0.003	3.06	±	0.149
EPP11-04	J0140	100	1.42	5.91	1.83	1.018	±	0.003	3.09	±	0.15
EPP11-05	J0141	110	1.39	6.60	1.95	1.053	±	0.003	3.14	±	0.15
EPP11-06	J0142	114	1.36	7.09	2.25	1.114	±	0.003	3.21	±	0.15
EPP11-07	J0143	118	1.39	7.33	2.26	1.145	±	0.003	3.27	±	0.15
EPP11-08	J0144	118	1.36	7.38	2.30	1.143	±	0.003	3.25	±	0.10
EPP11-09	J0145	128b	1.35	6.86	2.19	1.093	±	0.003	3.16	±	0.10
EPP11-10	J0146	128b	1.451	7.209	2.513	1.190	±	0.003	3.35	±	0.10
EPP11-11	J0147	128d	1.428	7.673	2.803	1.230	±	0.003	3.41	±	0.10

Table 2. Dose rate information for some El Paso Peaks samples, determined using in situ gamma spectrometry. The difference between the total dose rate for quartz and feldspar is due to the internal dose rate of K-feldspar that arises from the potassium.

Table 3

SAR sequence for quartz OSL measurements

Step	Description	Symbol
1	Give dose[a], D_i	
2	Preheat to 220°C for 10 s at 10°C s^{-1}	PH1
3	Stimulate with IR diodes at 60°C for 40 s (10°C s^{-1}, 90% power)	
4	Stimulate with blue LEDs (OSL) at 125°C for 40 s (10°C s^{-1}, 90% power)	L_N or L_x for regenerated doses
5	Give 10 s (1.15 Gy) test dose	D_T
6	Preheat to 200°C for 10 s at 10°C s^{-1}	PH2
7	Stimulate with IR diodes at 60°C for 40 s (10°C s^{-1}, 90% power)	
8	Stimulate with blue LEDs (OSL) at 125°C for 40 s (10°C s^{-1}, 90% power)	T_N or T_x for regenerated doses
9	Hot bleach at 220°C for 40 s	

[a] For the natural cycle, $i = 0$ and $D_0 = 0$ Gy.

Table 3. A typical SAR sequence used for quartz OSL measurements.

Table 4

Post-IR IRSL SAR measurement protocol

Step	Treatment	Measured
1	Give Dose[a], D_i	
2	Preheat[b] (250°C for 60 s)	ITL
3	Stimulate with IR diodes for 100 s at 50°C	IR_{50}; L_i
4	Stimulate with IR diodes for 100 s at 225°C	IR_{225}
5	Give test dose, D_t	
6	Preheat[b] (250°C for 60 s)	ITL
7	Stimulate with IR diodes for 100 s at 50°C	IR_{50}
8	Stimulate with IR diodes for 100 s at 225°C	IR_{225}; T_i
9	Hot bleach[c] at 290°C for 40 s	
10	Return to 1	

[a] For the natural cycle, $i = 0$ and $D_0 = 0$ Gy.

[b] In step 2 and 6, the TL signal can be observed, termed isothermal thermoluminescence (ITL).

[c] Hot bleach is used to remove any remaining charge (Wallinga et al., (2007).

[d] L_i and T_i are derived from the initial OSL signal (0.8 s) minus the background estimated from the last part of the stimulation curve (8 s).

Table 4. The post-IR IRSL measurement protocol of Buylaert et al. (2009). This protocol allows for three different signals to be observed: the signal arising during the preheat (the isothermal thermoluminescence (ITL) signal), the signal arising from IR stimulation at 50°C (the IR_{50} signal), and the signal arising from IR stimulation at 225°C (the IR_{225} signal).

Table 5

Luminescence dating results

Field code	Laboratory code	Depth (cm)	Quartz OSL (years before 2012)	Feldspar IRSL (60°C) (years before 2012)	Feldspar ITL (years before 2012)	Feldspar IRSL (50°C) (years before 2012)	Feldspar IRSL (225°C) (years before 2012)
Christmas Canyon West							
CCW-11-05	J0120	8	110 ± 70	110 ± 10	200 ± 50	190 ± 10	220 ± 10
CCW-11-01	J0116	14	250 ± 60	250 ± 20	210 ± 20	510 ± 30	780 ± 120
CCW-11-02	J0117	28	220 ± 200	480 ± 40	1200 ± 60	1190 ± 70	1840 ± 110
CCW-11-03	J0118	49	370 ± 70	890 ± 60	1120 ± 60	1570 ± 90	2800 ± 140
CCW-11-04	J0119	72	570 ± 110	1600 ± 80	2080 ± 110	2390 ± 140	3050 ± 160
Field code	**Laboratory code**	**Unit**	**Radiocarbon age range for sample[a]**	**Quartz OSL (years before 2012)**	**Feldspar ITL (years before 2012)**	**Feldspar IRSL (50°C) (years before 2012)**	**Feldspar IRSL (225°C) (years before 2012)**
El Paso Peaks							
EPP-11-01	J0137	90	50 - 400		1580 ± 110	740 ± 80	610 ± 50
EPP-11-02	J0138	92	50 - 400		1770 ± 130	730 ± 70	610 ± 60
EPP-11-03	J0139	98	50 - 510		1490 ± 110	950 ± 60	1830 ± 120
EPP-11-04	J0140	100	190 - 510	140 ± 60	420 ± 190	1050 ± 80	540 ± 480
EPP-11-05	J0141	110	350 - 580	110 ± 90	720 ± 170	810 ± 160	1600 ± 310
EPP-11-06	J0142	114	490 - 890	-70 ± 50	780 ± 60	190 ± 190	-150 ± 620
EPP-11-07	J0143	118	710 - 1590	20 ± 60	870 ± 250	1160 ± 80	2150 ± 230
EPP-11-08	J0144	118	710 - 1590	10 ± 20	1430 ± 80	1030 ± 60	1840 ± 220
EPP-11-09	J0145	128b	890 - 1590	30 ± 20	1510 ± 60	1920 ± 110	1870 ± 180
EPP-11-10	J0146	128b	890 - 1590		1880 ± 100	1790 ± 80	2400 ± 100
EPP-11-11	J0147	128b	890 - 1590		1690 ± 90	890 ± 40	1490 ± 100

[a] Radiocarbon age ranges from Dawson et al. (2003)

Table 5. Luminescence age results for CCW and EPP. Radiocarbon age ranges are calculated from Dawson et al. (2003) (see Table 6).

Table 6
Summary of radiocarbon chronology from Dawson et al. (2003)

Sample	Laboratory Code	Unit	Radiocarbon age, years	Calibrated age (2-σ)	Layer date posterior (2-σ)
EPP-1E-53b	Beta-82884	26a	150 ± 60	A.D. 1665-1920	not in analysis
EPP-1E-53a	AA17847	26a	2 ± 45	A.D. 1660-1960	A.D. 1670-1710, 1720-1820
EPP-1W-23	AA17842	94	320 ± 55	A.D. 1450-1660	not in analysis
EPP-1E-119	AA17838	98	225 ± 45	A.D. 1520-1590, 1620-1700, 1720-1880, 1910-1960	A.D. 1610-1710, 1720-1820
EPP-1E-30	AA17848	102	345 ± 50	A.D. 1440-1650	A.D. 1500-1660
Event W					A.D.1460-1630
EPP-1E-50	AA17837	110	431 ± 46	A.D. 1400-1530, 1560-1630	A.D. 1440-1530, 1550-1620
EPP-1W-70	AA17849	112	375 ± 40	A.D.1440-1640	A.D. 1425-1520
EPP-1W-20	Beta-82886	114	510 ± 60	A.D. 1290-1490	A.D. 1300-1370, 1380-1470
EPP-1W-116	AA17841	118	710 ± 95	A.D. 1060-1090, 1120-1140, 1150-1430	A.D. 1120-1140, 1150-1420
Event U					A.D. 450-1300
EPP-1W-71	AA17834	132	1675 ± 50	A.D. 240-440, 450-470, 520-530	not in analysis
EPP-1W-15	AA17843	138	1540 ± 50	A.D. 420-640	A.D. 420-640
Event Q/R					A.D. 40-550
EPP-1W-31	AA17835	164	1930 ± 45	50 B.C.-A.D.220	50 B.C.-A.D. 180, A.D.190-220
EPP-1W-25	AA17850	166	2735 ± 65	1020-790 B.C.	1030-790 B.C
EPP-1W-36	AA17839	190	3700 ± 50	2280-2250, 2210-1940 B.C.	2130-1910 B.C.
EPPT2-21	AA34429	192	3735 ± 45	2290-2020, 2000-1970 B.C.	2210-2020 B.C.
EPP-1W-30	AA17852	192	3680 ± 40	2200-2160, 2150-1940 B.C.	2200-2160, 2150-1970 B.C.
EPP-1E-45	AA17854	198	3740 ± 40	2290-2020, 2000-1980 B.C.	2290-2060 B.C.
EPP-1W-14	AA17856	214	3905 ± 50	2560-2530, 2500-2200 B.C.	2470-2270, 2260-2200 B.C.
EPPT2-26	AA34430	216	3975 ± 50	2620-2300 B.C.	2585-2401 B.C.
EPP-1E-57	AA17840	216	3945 ± 55	2580-2280 B.C.	2580-2330 B.C.
EPPT2-63	AA34432	218	4320 ± 45	3090-3060, 3040-2870 B.C.	2630-2340 B.C.
EPP-1E-105	Beta-82885	K fissure	4610 ± 80	3524-3090 B.C.	not in analysis
EPP-1E-103	AA21661	K fissure	4535 ± 55	3487-3047 B.C.	not in analysis
EPP-1E-108	AA17846	K fissure	4490 ± 60	3369-3080, 3067-3030 B.C.	not in analysis
EPP-1E-98	AA21660	236	4515 ± 55	3370-3020 B.C.	3250-3000, 2990-2920 B.C.
EPP-1E-106	AA17836	236	4410 ± 55	3340-3210, 3190-3150, 3130-2900 B.C.	3190-3150, 3140-2910 B.C.
Event k					3330-3050 B.C.
EPPT2-65	AA34433	240	4520 ± 45	3370-3080, 3060-3030 B.C.	3360-3120 B.C.
EPPT2-53	AA33517	254	4515 ± 60	3500-3450, 3400-2950 B.C.	3500-3460, 3380-3170 B.C.
EPPT2-80	AA34434	316	5420 ± 55	4360-4040 B.C.	4360-4040 B.C.
Event F					5300-4200 B.C.
EPPT2-92	AA34435	374	6225 ± 75	5340-4950 B.C.	5340-4950 B.C.

Table 6. Summary of the radiocarbon chronology at El Paso Peaks from Dawson et al. (2003). The maximum and minimum age (layer date posterior) of samples that bracket the luminescence samples in this study were used to calculate a target age range for the luminescence samples.

Table 7

Selective SAR48-12 age estimates

Sample	Signal	Initial age estimate	SAR48-12 age estimate	Target age range
J0140	IR_{50}	1050 ± 80	375 ± 27	190 - 510
	IR_{225}	540 ± 480	579 ± 41	190 - 510

Table 7. Initial feldspar IRSL age estimates compared to age estimates derived using the selective SAR48-12 method, developed as a method to isolate the 12 out of 48 aliquots with the lowest D_e values, which are presumably the most well bleached.

Table 8

Fading rates using the long method

	g value (%/decade)		
Sample code	ITL	IR_{50}	IR_{225}
J0137	-1 ± 2	1 ± 1	-2 ± 2
J0138	6 ± 2	3 ± 2	2 ± 3
J0139	-4 ± 4	1 ± 2	3 ± 2
J0146	7 ± 1	5 ± 1	3 ± 1
J0147	5 ± 2	4 ± 1	-2 ± 3
J0148	7 ± 0	12 ± 12	-68 ± 69
J0149	3 ± 15	1 ± 20	17 ± 25

Table 8. Fading rates (g values) obtained using by comparing the initial IRSL intensity to that after the sample had been irradiated and store for some length of time (i.e. 2 days).

Table 9

Fading rates (g values; %/decade) calculated using the quick fade method

a. ITL after pause

	J0141						J0142					
	Disc 1			Disc 2			Disc 1			Disc 2		
ITL	8	±	6	33	±	8	15	±	6	27	±	7
IR50	-1	±	6	34	±	11	26	±	21	1	±	9
IR225	-3	±	7	16	±	12	-5	±	21	4	±	9

b. TL before pause

	J0141						J0142			J0144		
	Disc 1			Disc 2			Disc 1			Disc 1		
IR50	12	±	12	13	±	10	41	±	7	11	±	6
IR225	11	±	12	10	±	11	12	±	19	-6	±	8

Table 9. Fading rates (g values) obtained using the "quick fade" method, in which aliquots are given a dose and then re-measured after five different (short) delay times. The g values obtained for different discs of the same sample are shown to illustrate the high degree of variation.

Table 10

Single-grain feldspar IRSL measurements

Sample	IR_{50}	IR_{225}	Radiocarbon age range for sample
J0140	470 ± 100	450 ± 180	190 - 510
J0143	390 ± 50	550 ± 60	710 - 1590
J0145	840 ± 90	1110 ± 90	890 - 1590

Table 10. Raw (fading uncorrected) single-grain feldspar IRSL measurements made on samples J0140, J0143 and J0145.

Table 11

IRSL D_e values and age estimates before and after the quick HF treatment

		Before HF De	After HF De	Before HF	After HF age	Target age (years before present)
J0141	ITL	2.25 ± 0.53	3.65 ± 0.16	720 ± 170	1164 ± 75	582 - 342
	IR50	2.54 ± 0.47	1.55 ± 0.23	810 ± 160	494 ± 77	
	IR225	5.01 ± 0.95	3.10 ± 0.17	1600 ± 310	988 ± 72	
J0142	ITL	2.51 ± 0.17	3.03 ± 0.24	780 ± 60	944 ± 86	982 - 432
	IR50	0.62 ± 0.62	1.63 ± 0.20	190 ± 190	508 ± 66	
	IR225	-0.49 ± 1.99	2.55 ± 0.34	-150 ± 620	794 ± 112	
J0144	ITL	4.63 ± 0.21	3.38 ± 0.29	1430 ± 80	1042 ± 95	1472 - 552
	IR50	3.34 ± 0.18	2.19 ± 0.21	1030 ± 60	675 ± 68	
	IR225	5.98 ± 0.68	2.93 ± 0.32	1840 ± 220	903 ± 103	

Table 11. Single-grain feldspar IRSL measurements made on samples J0140 and J0145. Because of the identification of an iron coating on many feldspar grains, a quick HF treatment in an attempt to the outer part of the grains. Re-measurement of these samples showed a significant increase in IRSL intensity, however, there appears to be no systematic improvement in the age estimates.

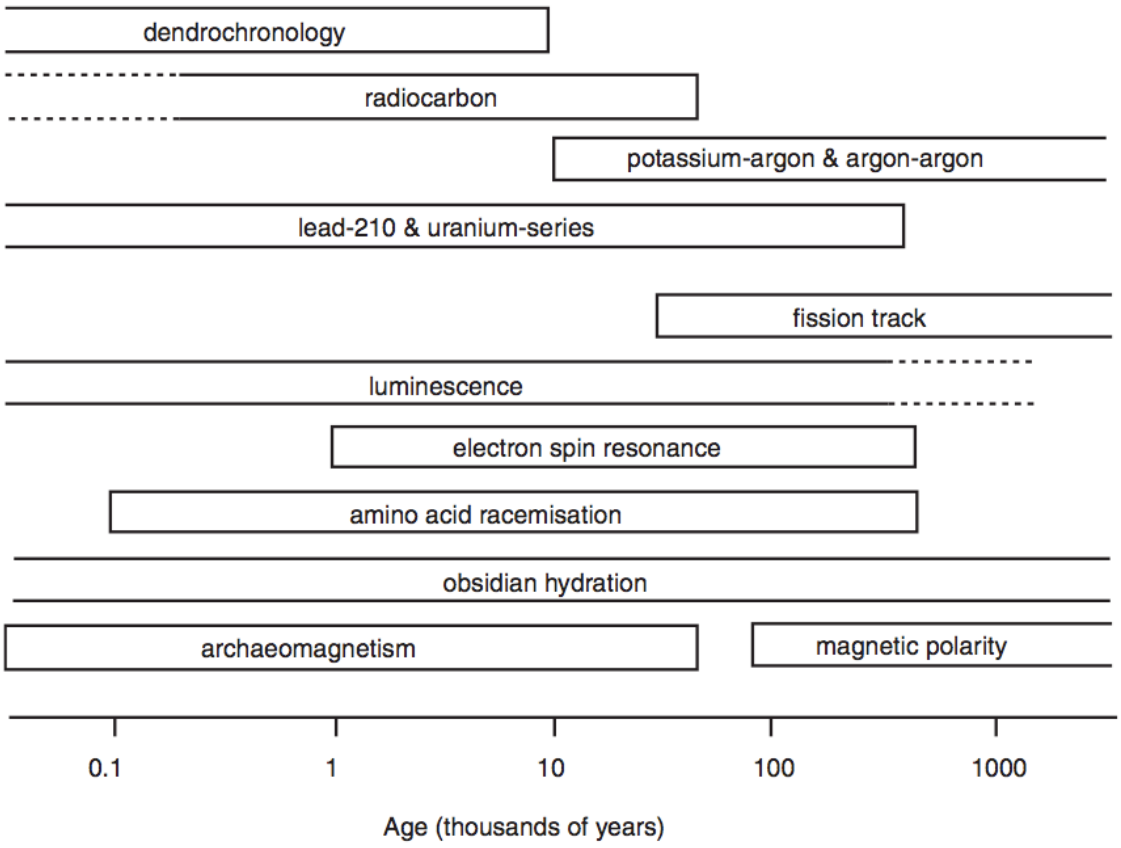

Figure 1. Age ranges of some Quaternary dating methods. Most methods are limited by the presence of specific material that has to occur in a relevant context. Many of these methods are only applicable over short timescales, calculated ages may not directly date the event of interest, and complex age calibration may be required, which may greatly increase uncertainties. Luminescence is an advantageous dating method in that it can be applied to ubiquitous materials, directly dates the depositional event of interest, can be applied to a wide range of ages, and gives calendar ages that do not require complex calibrations (after Lian and Roberts, 2006).

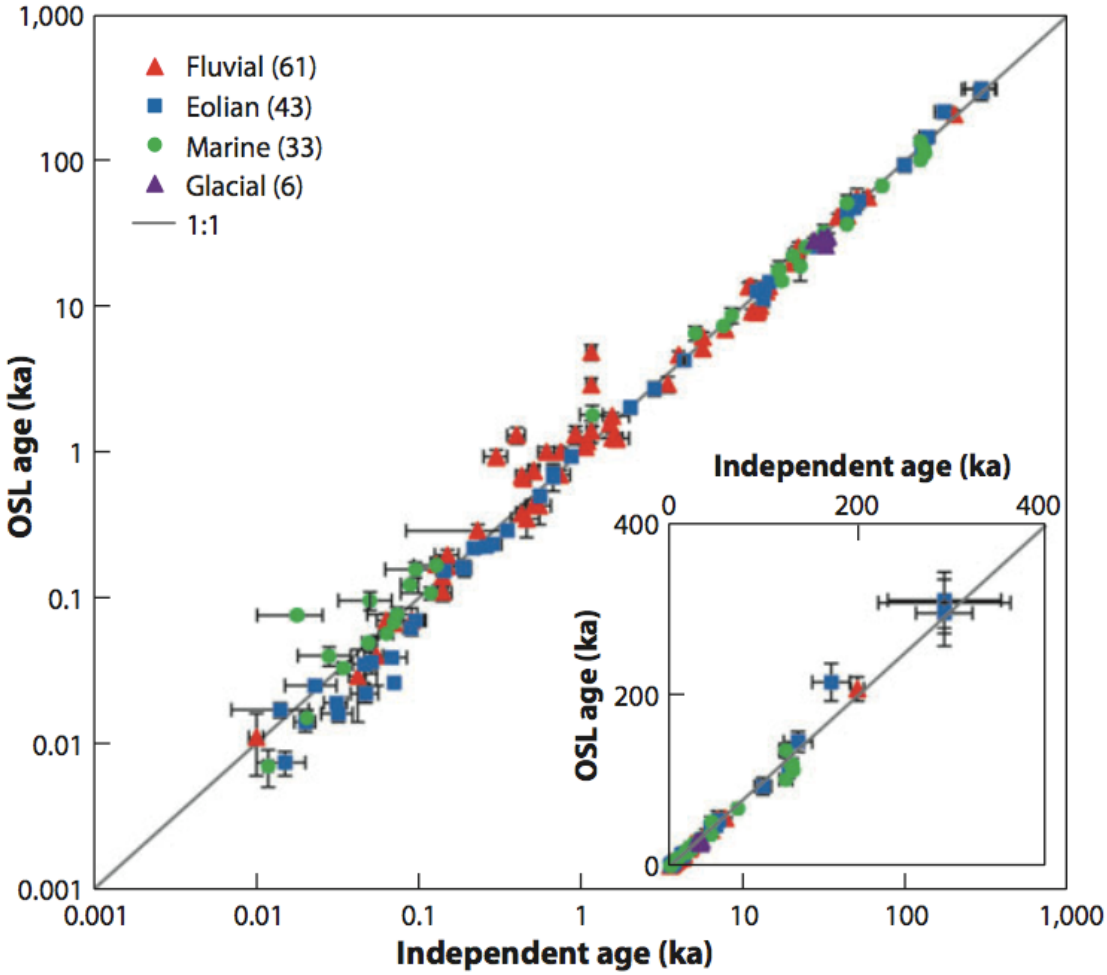

Figure 2. Good agreement has been found between quartz SAR OSL ages and independent chronological control for 143 samples from fluvial, eolian, marine and glacial contexts. The solid represent agreement between methods, and while some samples lie above the line (representing age overestimates thought to be the product of incomplete bleaching), most samples indicate good agreement. This consistency between OSL ages and independent age controls indicates the good performance of quartz SAR protocols for age determination (after Rhodes, 2011).

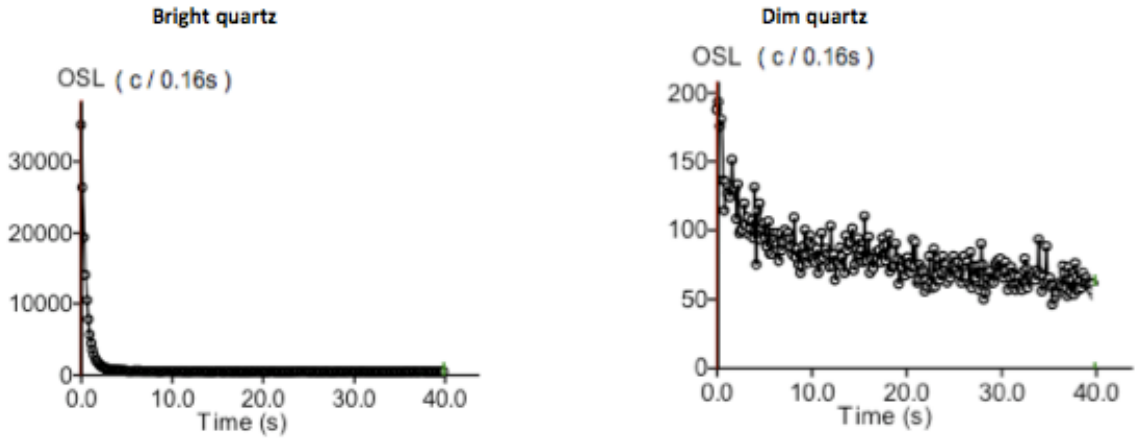

Figure 3. Natural OSL decay curves for bright quartz (left) from a cliff-top dune in Malibu, California, and dim quartz (right) from the Christmas Canyon West site in the Mojave Desert. Bright quartz is characterized by high intensity (high number of luminescence counts per 0.16s, y-axis) and a rapidly decaying signal, often yielding accurate and precise age estimates using a SAR protocol. Dim quartz, on the other hand, has significantly lower signal intensity and a slowly decaying signal, and are typically not suitable for accurate age determinations using a conventional SAR protocol. (Figure drafted by Ed Rhodes)

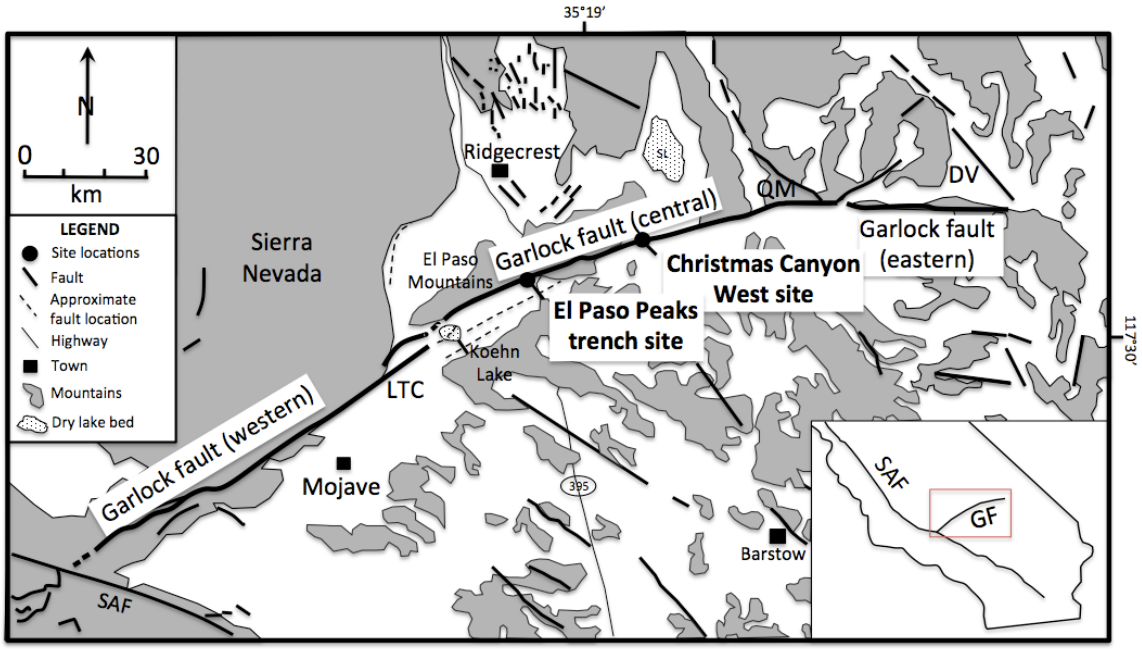

Figure 4. Location map of the Garlock fault, El Paso Peaks trench site and Christmas Canyon West site, California. Shaded regions denote mountains, open regions are valleys. Red box within the inset shows this map area in relation to southern California. SAF is San Andreas fault, GF is Garlock fault, LTC is Lone Tree Canyon, SL is Searles (dry) Lake, QM is Quail Mountain, DV is Death Valley. Modified from

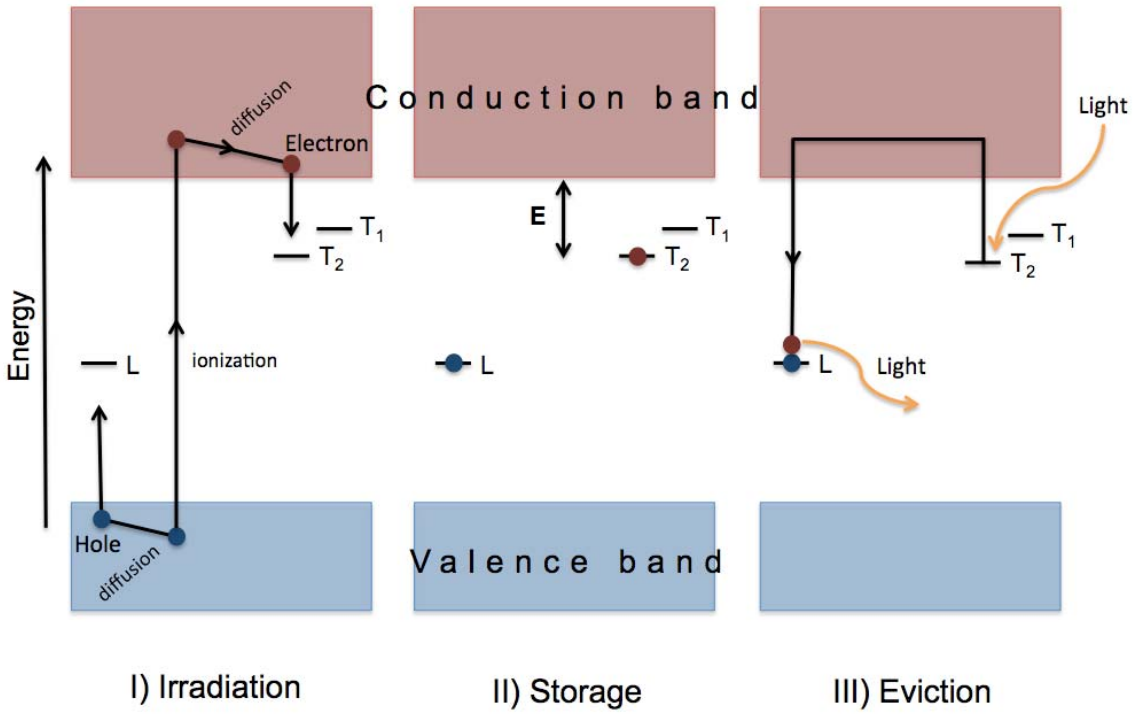

Figure 5. Energy level diagram illustrating the process of luminescence: I) ionizing radiation interacts with the mineral grains, causing electrons to be excited from their stable valence band position into the conduction band, leaving holes in the valence band; II) electrons become trapped at defect sites (T_1, T_2, etc.); III) mineral grains are stimulation by heat or light, causing electrons to be released from traps and recombine at luminescence centers (L), emitting light photons (i.e. the luminescence signal). Reproduced from Duller (2008).

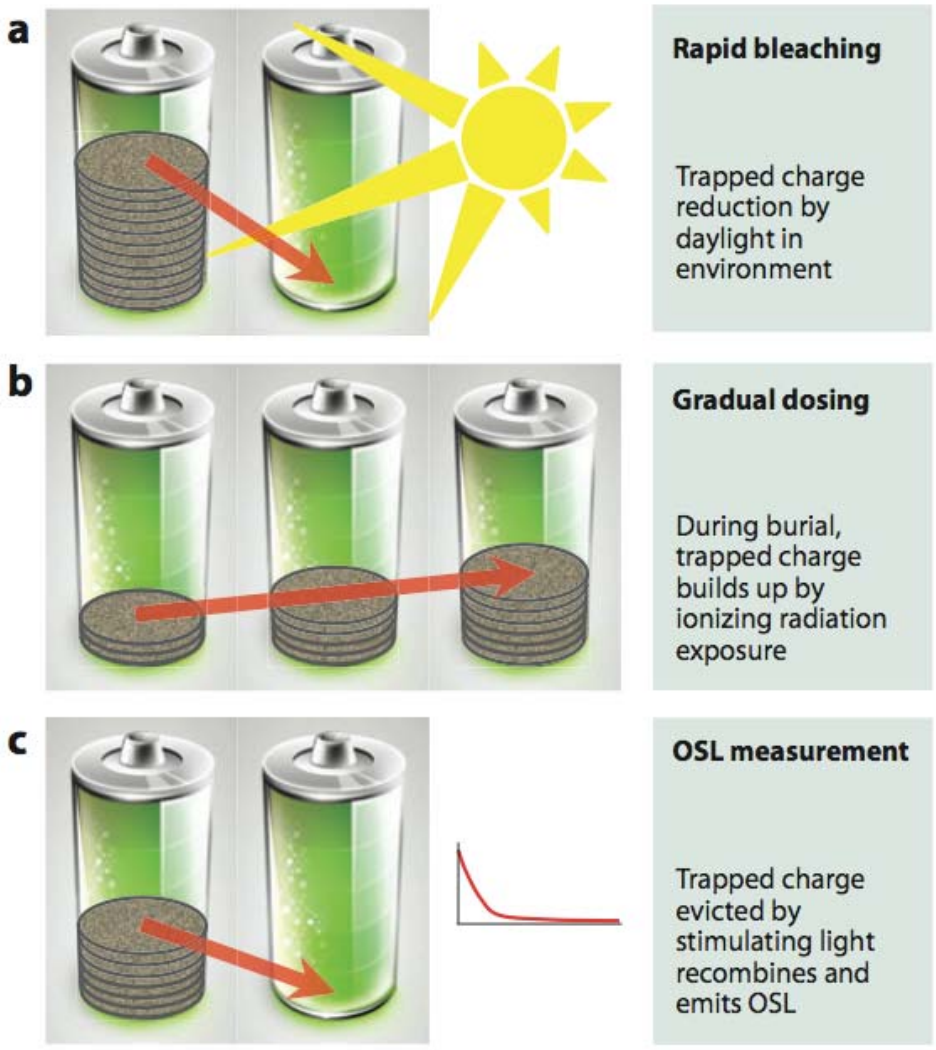

Figure 6. The analogy of a rechargeable battery forms a useful analogy for how luminescence dating works. a) When mineral grains are exposed to sunlight or heat during transportation, trapped electrons are leased, similar to depleting a battery of its charge. b) When exposure to sunlight or heat ceases (i.e. deposition and burial), re-exposure to environmental radiation causes charge to build up, much like recharging a battery. c) After sample collection, mineral grains are stimulated by light or heat in the laboratory, releasing the stored energy in the form of light, which is measured as the luminescence signal (after Rhodes, 2011).

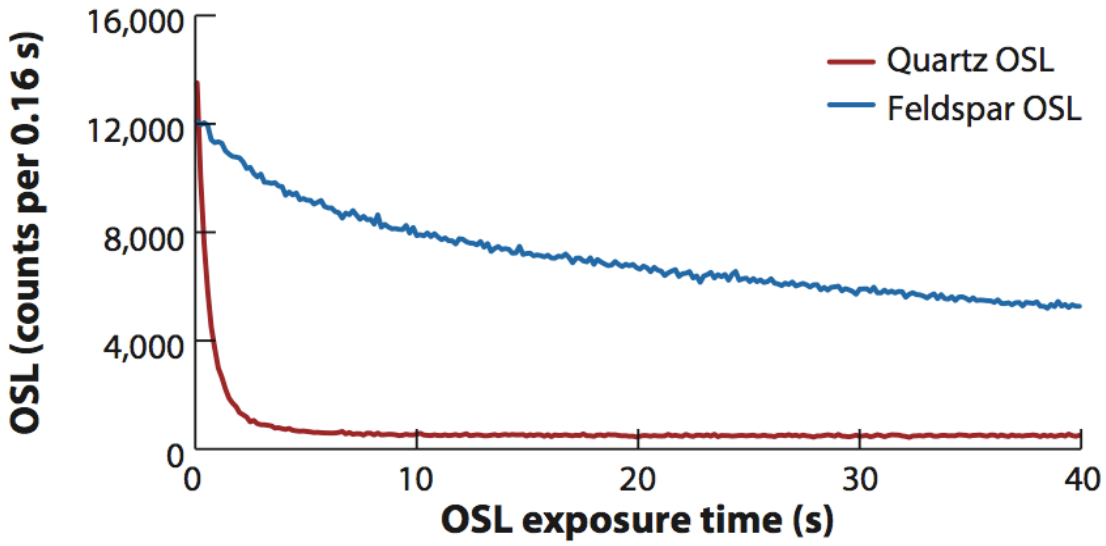

Figure 7. Decay curves quartz OSL and feldspar IRSL. Note the different shape of the decays for the two minerals. This difference in the shape of the decay curves can be used to test for feldspar contamination in quartz OSL measurements (after Rhodes, 2011).

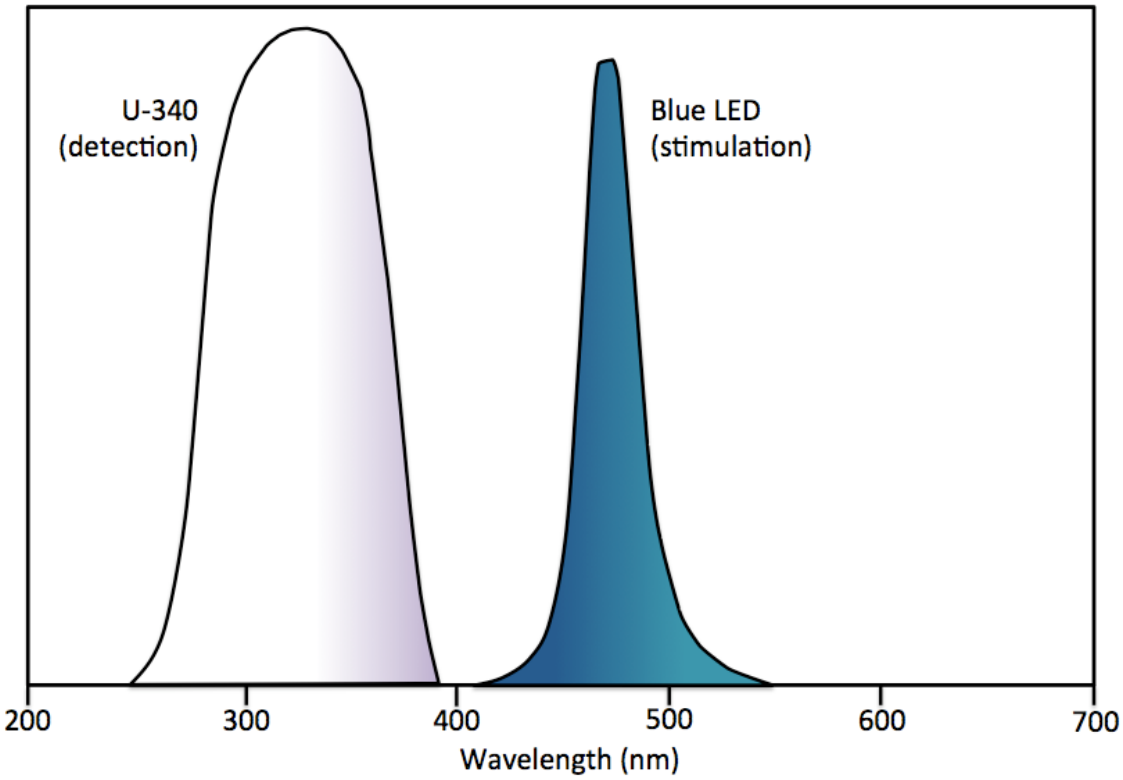

Figure 8. When stimulating with blue LEDs (peak emission at 470 nm), a filter is necessary to block wavelengths of light coming from the stimulation source from reaching the photomultiplier tube, and allow only the light emitted as luminescence from the sample (quartz OSL has a peak emission of 365 to 380 nm). A Hoya U-340 filter will block wavelengths greater than 380 nm, but allows light from 280 to 380 nm to pass. Redrawn from Duller, 2008.

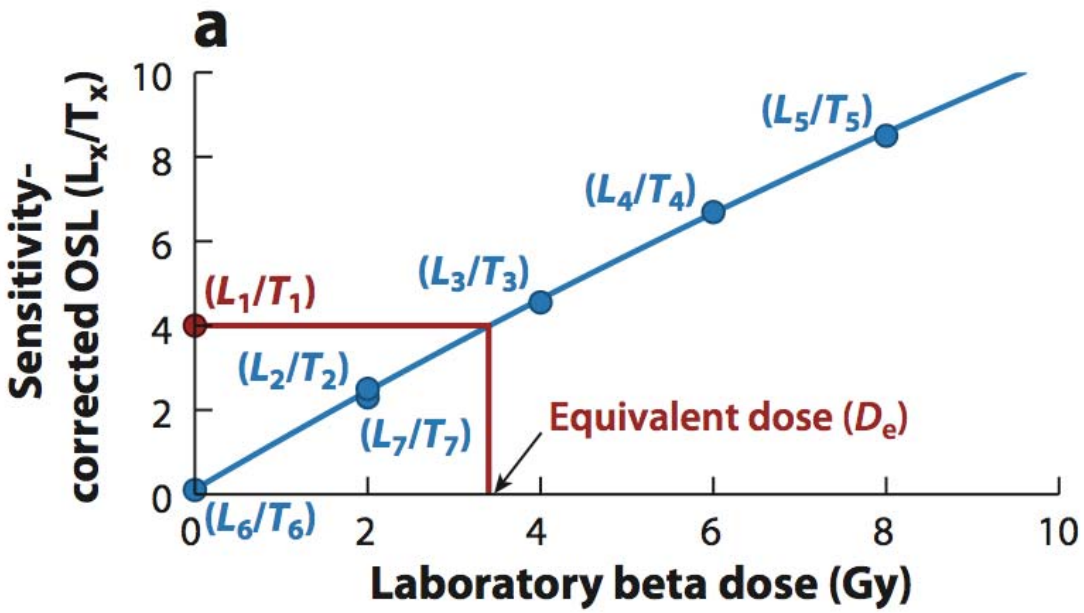

Figure 9. A growth curve used for equivalent dose (D_e) determination. During a typical single-aliquot regenerative dose (SAR) sequence, the natural or regenerative dose OSL (L_x) is corrected by the OSL response to a test dose (T_x). For each aliquot measured, the natural OSL (L_1/T_1) is compared to the growth curve created by the regenerative-dose OSL measurements (L_2/T_2, L_3/T_3, etc) to provide a D_e estimate (after Rhodes, 2011).

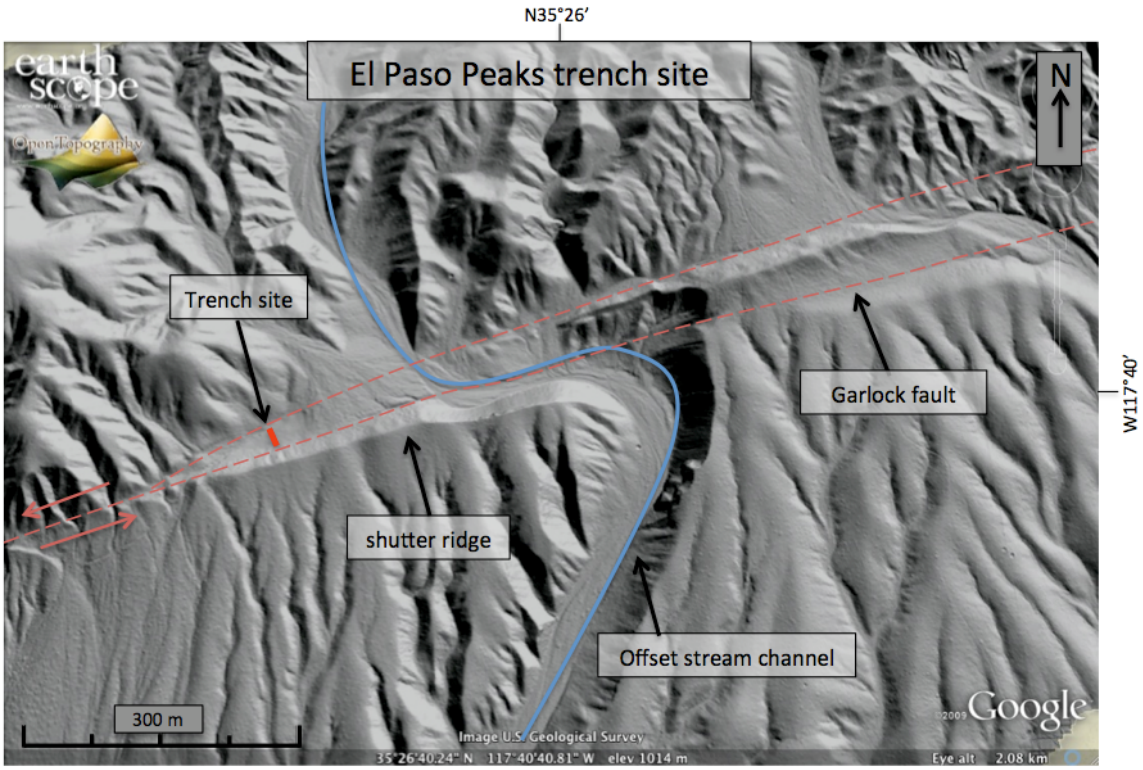

Figure 10. Overview of the El Paso Peaks trench site area. The trench site is located in a small playa that is bounded to the north by the El Paso Mountains, to the south by a shutter ridge, and to the east by a small Holocene alluvial fan, and is adjacent to a remarkably offset stream channel. The image comes from EarthScope's OpenTopography add-ins on Google Earth.

Figure 11. Sediments within the El Paso Peaks trench, composed mainly of graded sand and silt, with some gravels occurring near the top. These distinctive units are mostly laterally continuous and easy to correlate along the length of the trench, making this an ideal location for geochronological investigations.

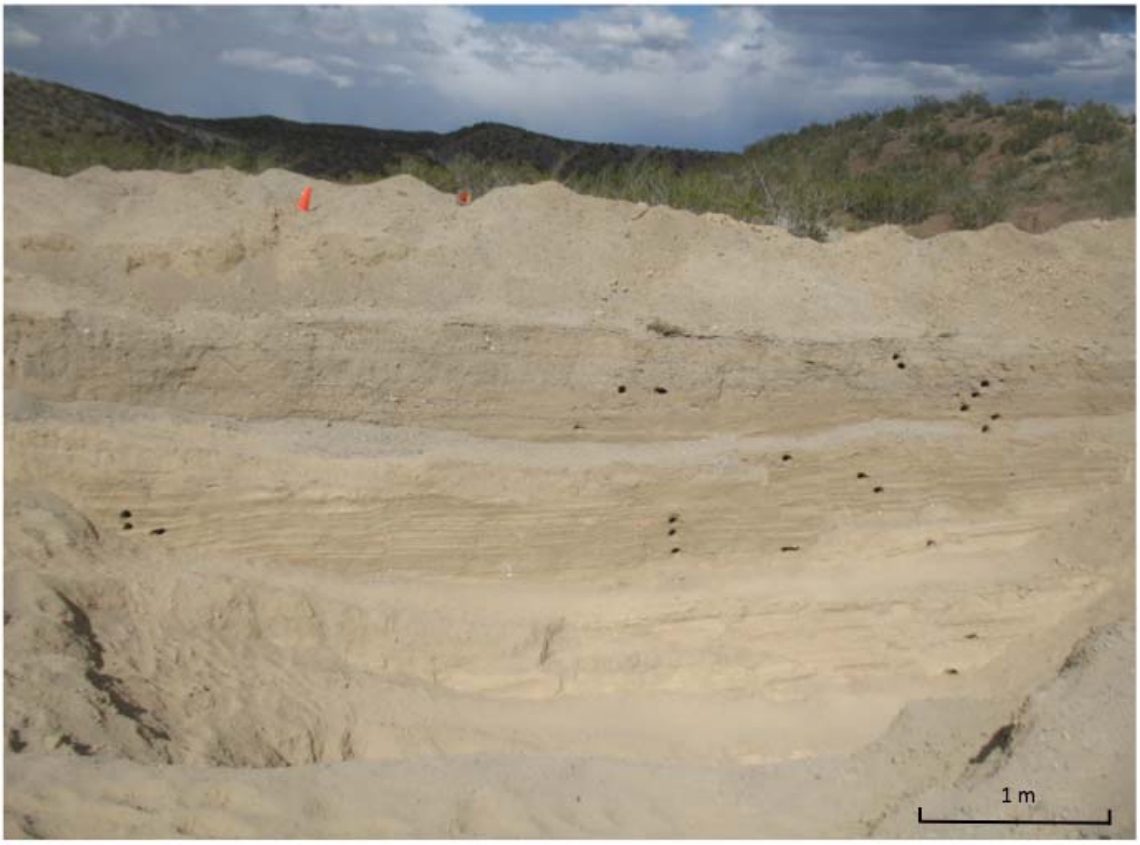

Figure 12. The El Paso Peaks trench (view to the east) from which samples were collected for luminescence dating. Holes are sample locations.

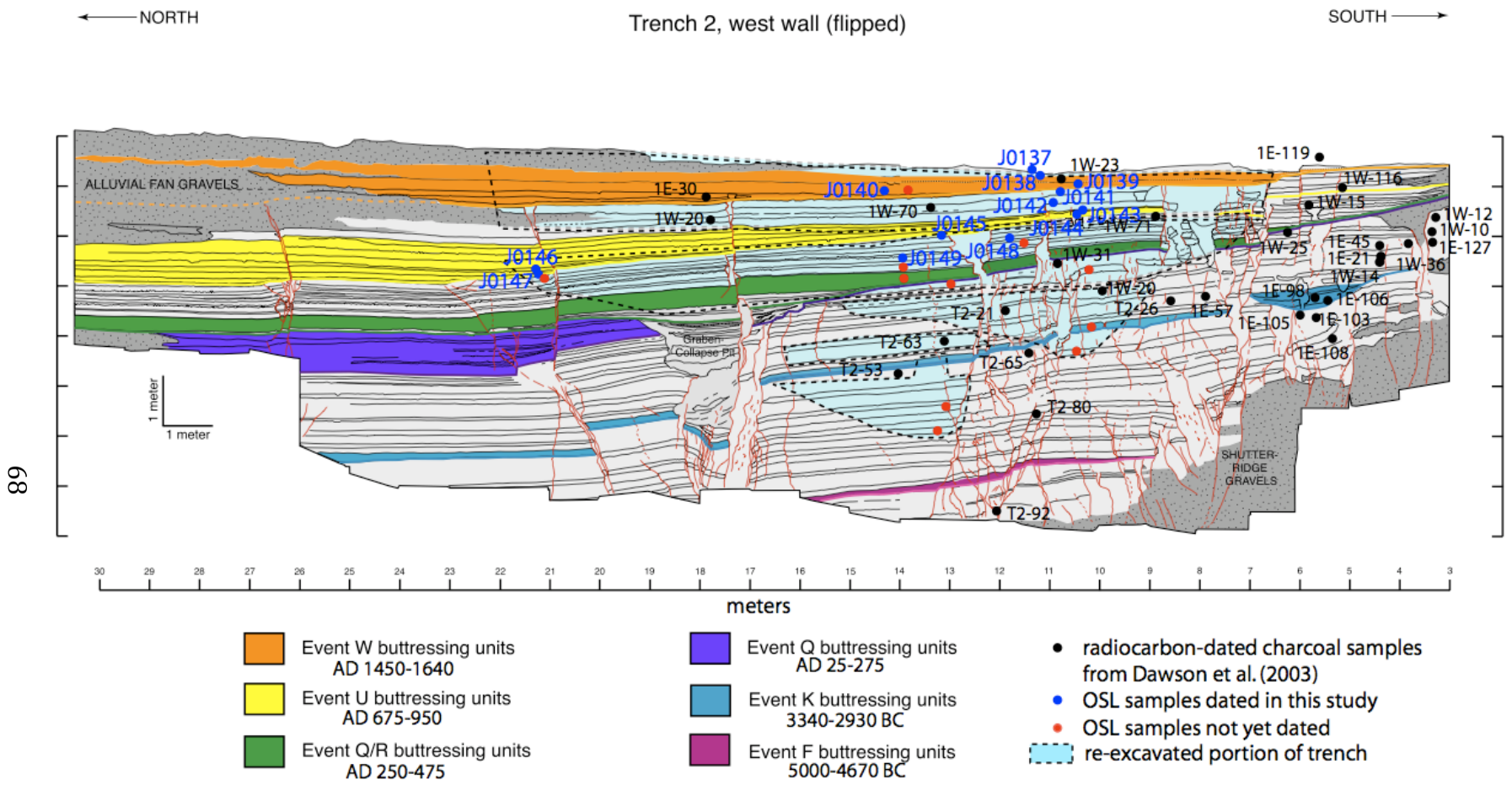

Figure 13. Trench log from Dawson et al. (2003), with the 2009 excavation superimposed, with radiocarbon and luminescence sample locations marked. Figure modified with help from Sally McGill.

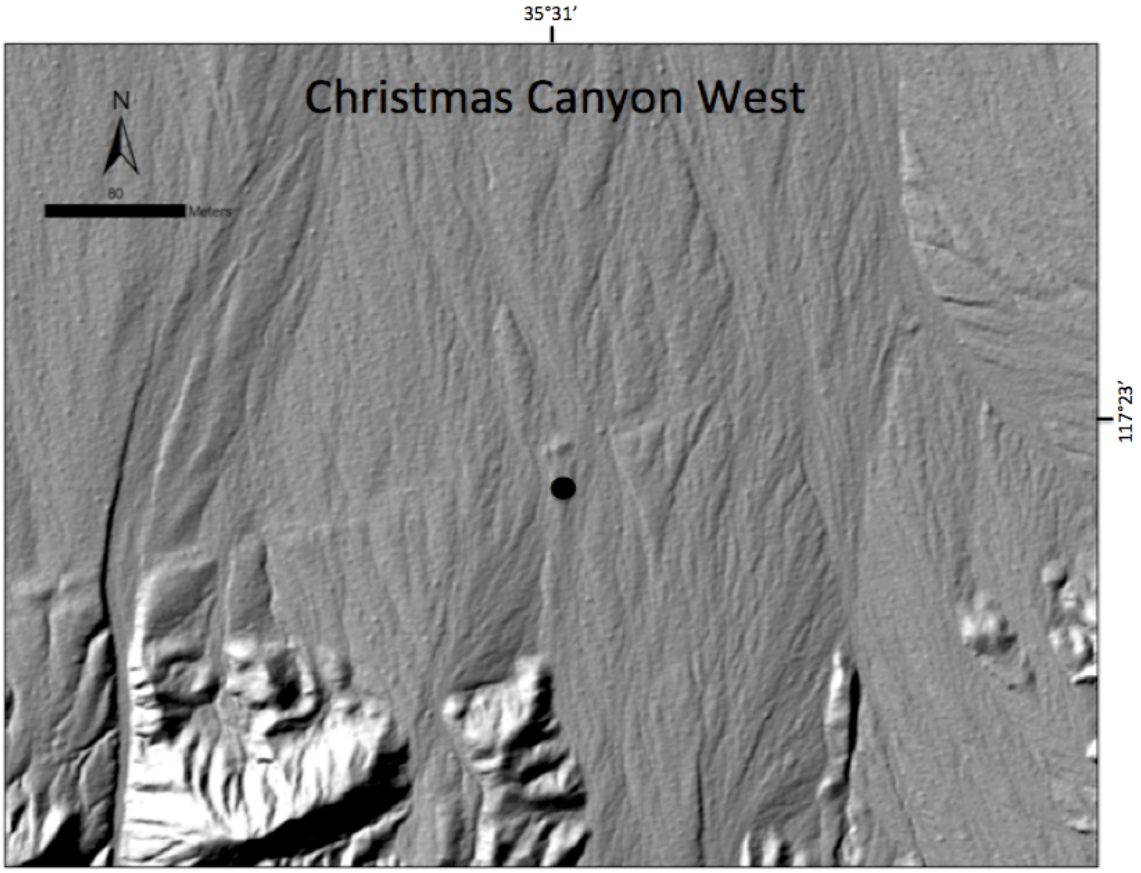

14. LIDAR image of the Christmas Canyon West site, located on the central Garlock fault. The black circle marks the sampling location. Note the fault trace running NE-SW. Offset alluvial fan features have been identified at this site, and future studies will obtain fault slip rates on this section of the Garlock fault using luminescence dating. Image courtesy of James Dolan and Lee McAuliffe, USC.

Figure 15. Sampling pit dug at Christmas Canyon West (CCW) for luminescence dating. Samples were collected in this pilot study to assess the luminescence characteristics of quartz and feldspar in this region. From this pit (approximately 1 m deep), 5 samples were collected for quartz OSL and feldspar IRSL dating. Note the sample tube in place in the upper right corner, and the portable gamma spectrometer collecting in situ dose rate information in the second to lowest sample location.

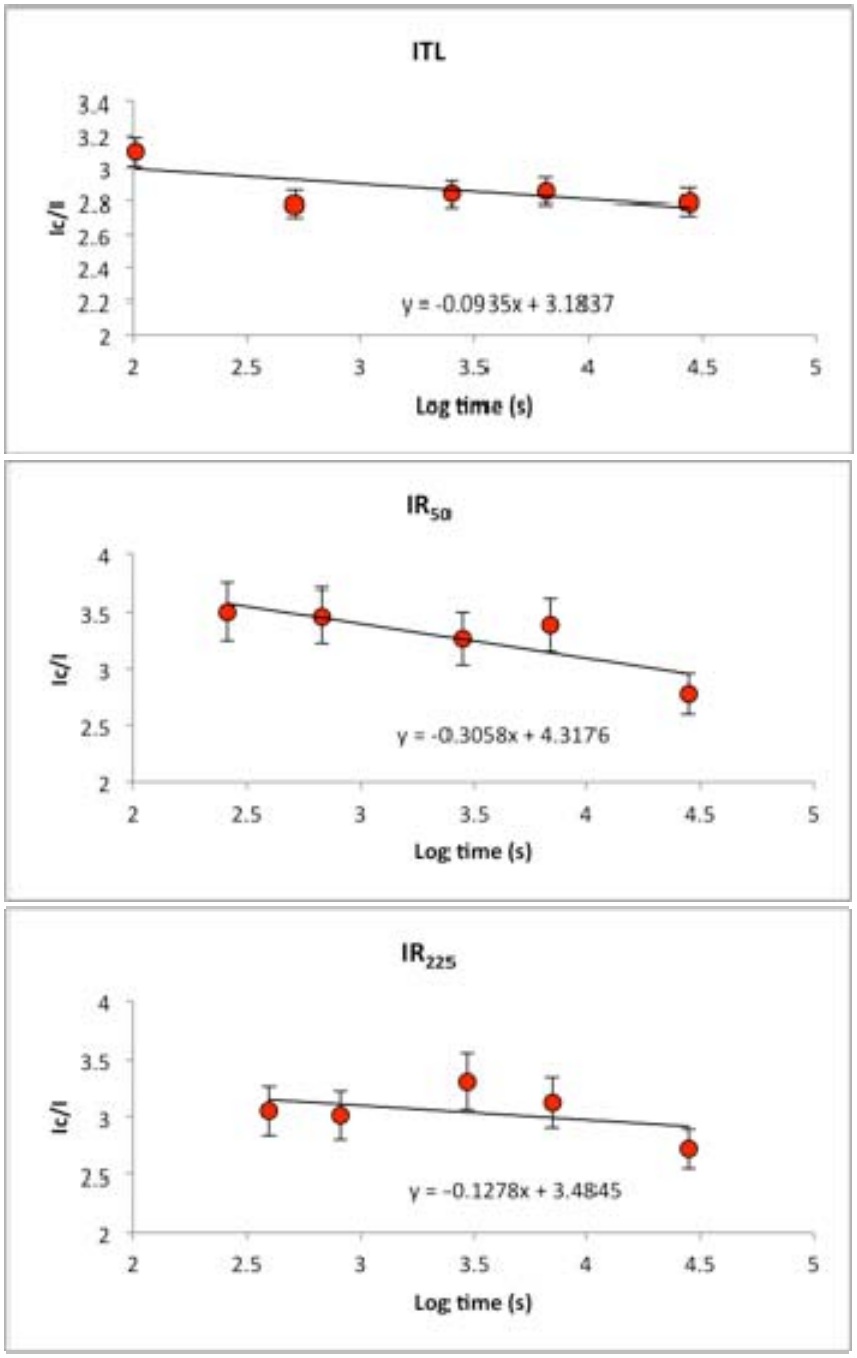

Figure 16. The "quick fade" method was developed in this study as a rapid method of obtaining fading rates, or g values, for feldspar IRSL dating. This method administers a fixed dose to each aliquot, and measures the IRSL signals after five different delay times (410 s, 1320 s, etc.). By plotting the IRSL intensities versus the log of time elapsed since irradiation, the g values can be deduced from the line connecting the points (Auclair et al., 2003).

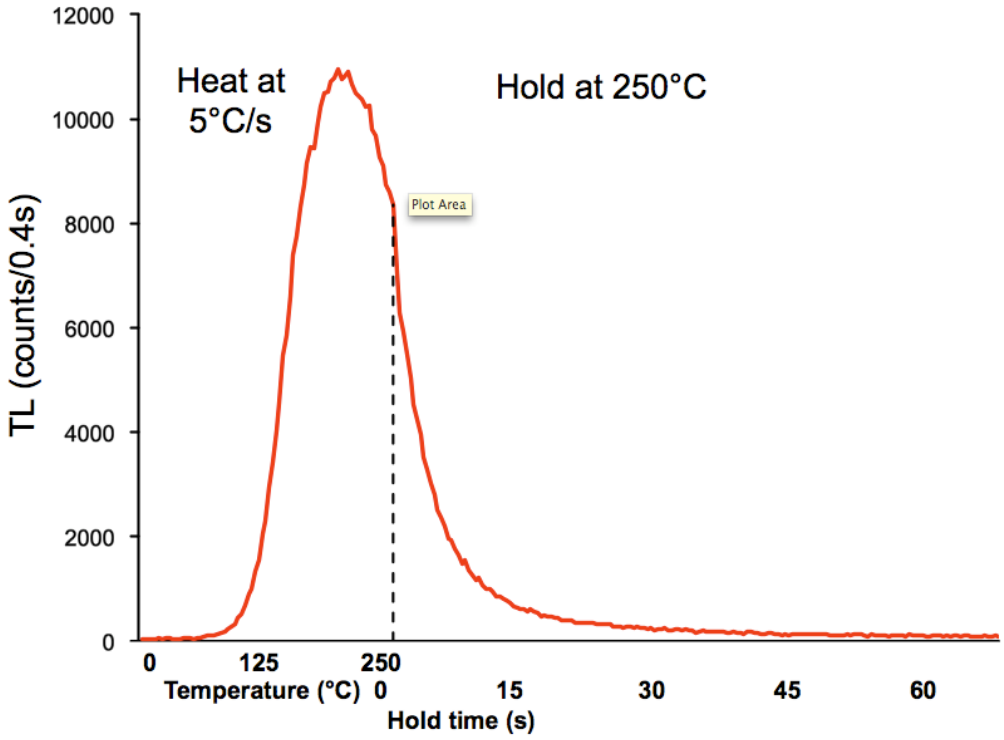

Figure 17. The novel feldspar isothermal thermoluminescence (ITL) approach, developed in this study, measures the ITL signal during the preheat of the SAR protocol. By heating the samples to 250°C and holding it there for 60 s, the resulting TL curve (above) can be treated as OSL or IRSL decay curve. Figure drafted by Ed Rhodes.

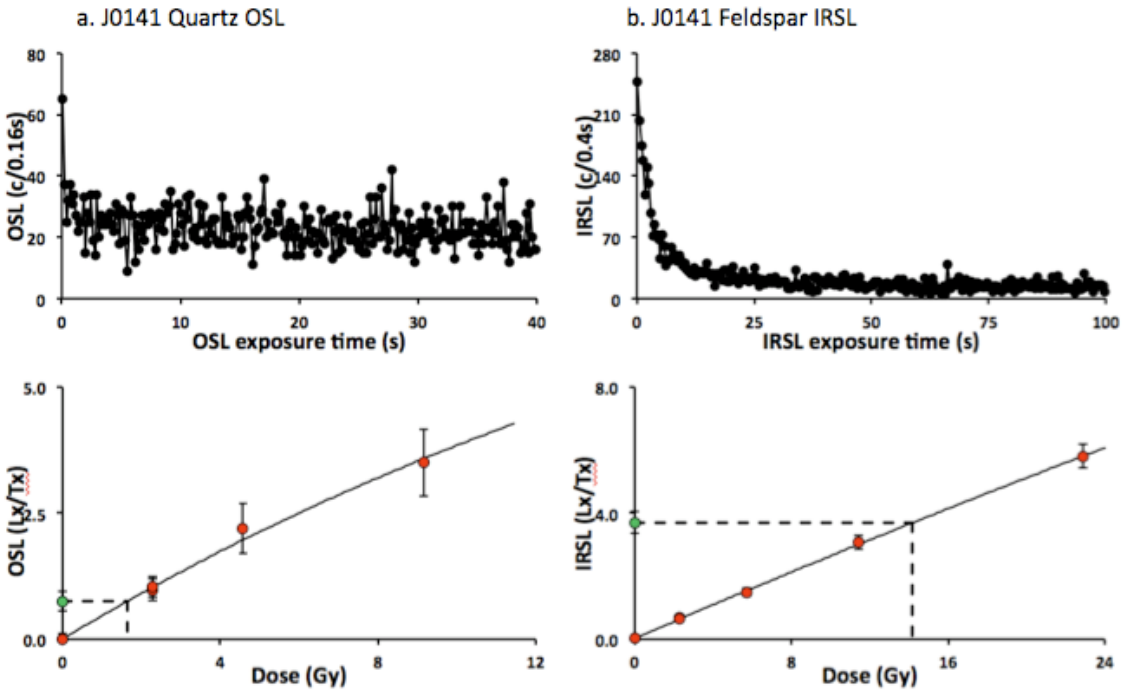

Figure 18. Decay curves (upper) and growth curves (lower) for sample J0141 (a.) quartz OSL and (b.) feldspar IRSL. Both minerals display low luminescence intensity, resulting in a dim signal. The quartz OSL decay curve is dominated by the medium and slow components, which is a limiting factor in the determination of precise age estimates.

Figure 19

Quartz OSL equivalent dose values for sample J0141

Aliquot number	Equivalent Dose (De)
1	**0.31 ± 0.31**
2	**0.32 ± 0.32**
3	0.47 ± 0.47
4	0.75 ± 0.75
5	0.85 ± 0.85
6	0.88 ± 0.88
7	1.21 ± 1.21
8	1.36 ± 1.36
9	1.42 ± 1.42
10	1.65 ± 1.65
11	2.14 ± 2.14
12	2.44 ± 2.44

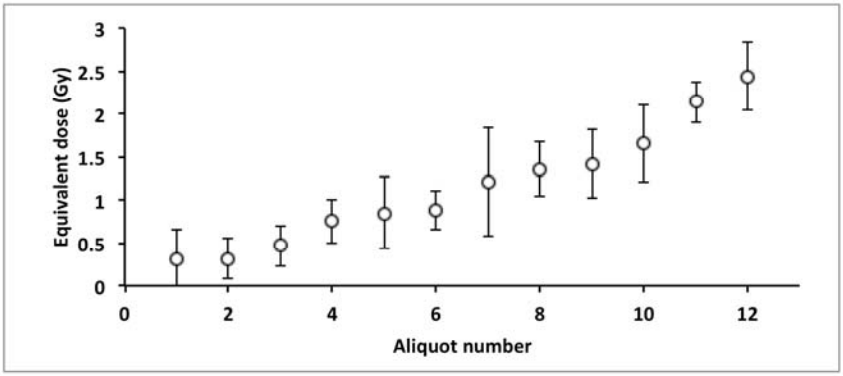

Figure 19. Equivalent dose (D_e) distribution for quartz OSL measurement on sample J0141. The high degree of variability between D_e values measured on each aliquot suggests a mixture of well-bleached grains and poorly bleached grains, which contain a residual signal resulting in an overestimate. This variation suggests that the lowest D_e values are the most well bleached, and free of any significant residual signal. Therefore, the lowest, consistent group of D_e values are used for age determination.

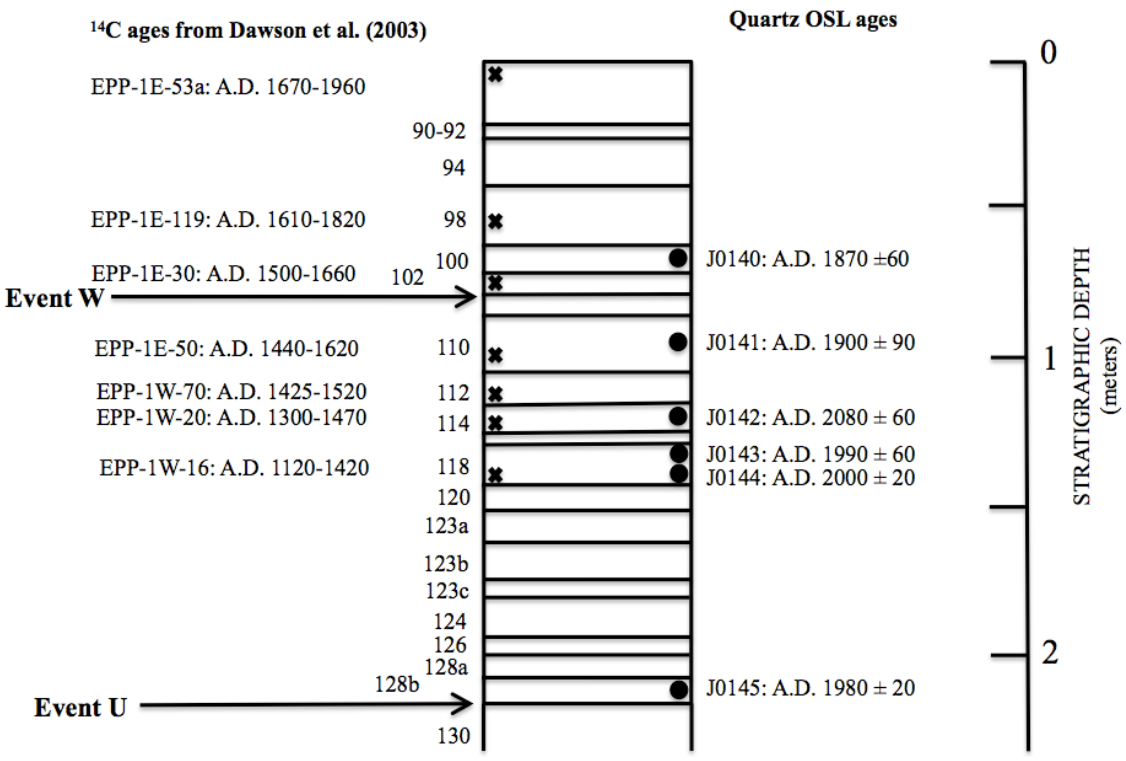

Figure 20. Simplified stratigraphic column of some El Paso Peaks samples. Numbers down the left side of the column indicate stratigraphic units. Quartz OSL age estimates have been converted into A.D.-B.C. form for easy comparison with the radiocarbon dates from Dawson et al. (2003). The quartz OSL age estimates are highly underestimated in comparison with the radiocarbon ages, and are not in stratigraphic order.

Figure 21

J0140 feldspar IRSL equivalent dose distributions using the SAR48-12 method

Aliquot number	IR_{50} equivalent Dose (De)
1	**0.93 ± 0.16**
2	**0.95 ± 0.55**
3	0.98 ± 0.13
4	1.00 ± 0.61
5	1.06 ± 0.18
6	1.19 ± 0.35
7	1.24 ± 0.11
8	1.33 ± 0.23
9	1.35 ± 0.21
10	1.42 ± 0.34
11	1.57 ± 0.14
12	1.57 ± 0.86

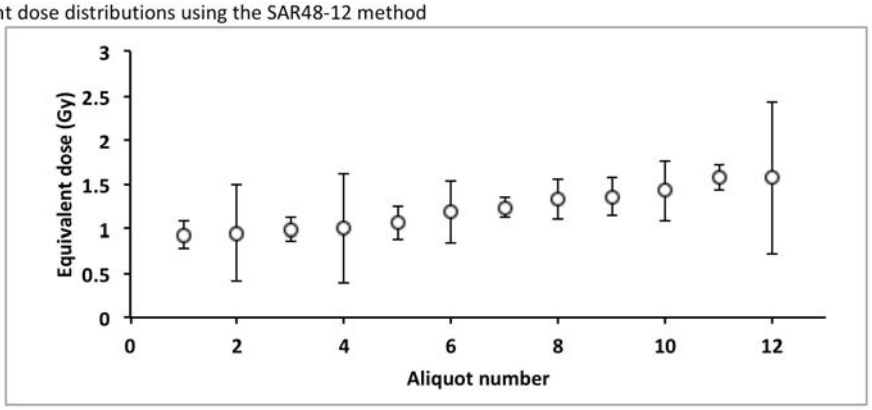

Aliquot number	IR_{225} equivalent Dose (De)
1	**1.32 ± 0.19**
2	**1.66 ± 0.14**
3	1.83 ± 0.20
4	1.91 ± 0.18
5	1.99 ± 1.37
6	2.11 ± 0.28
7	2.18 ± 0.37
8	3.13 ± 0.36
9	3.38 ± 0.21
10	3.41 ± 1.35
11	4.97 ± 0.20
12	23.29 ± 4.91

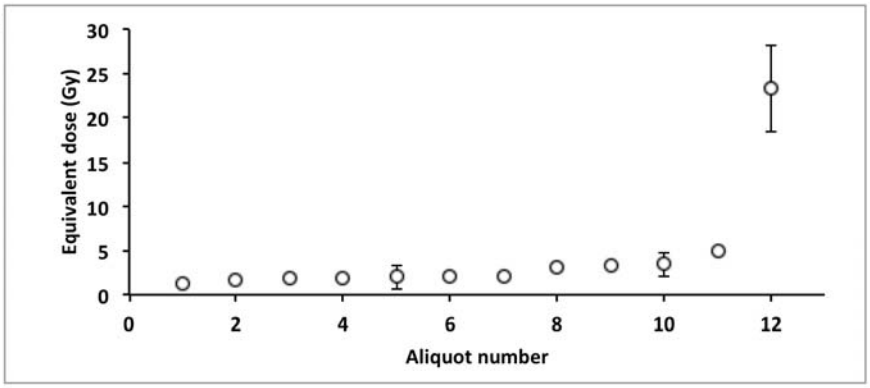

Figure 21. Equivalent dose distributions obtained using the SAR48-12 for J0140 feldspar. This method chooses 12 of 48 aliquots with the lowest D_e values, assuming they are the most well bleached, resulting in a less variable D_e distributions and more accurate age estimates.

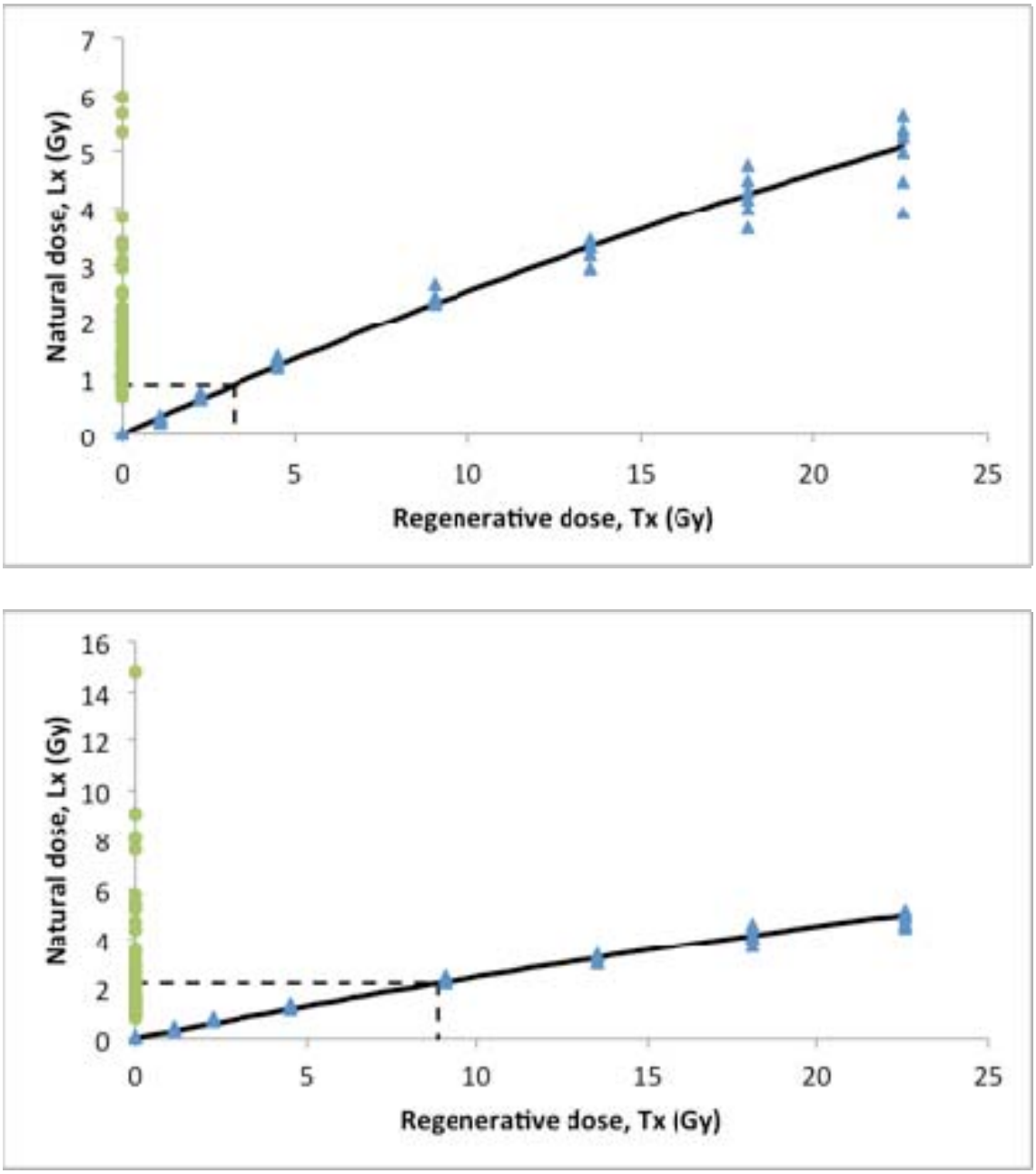

Figure 22. Combined growth curves for sample J0143 using the SACoR method. The natural luminescence measurement is plotted to the left in green, while the regenerative measurements are plotted in blue.

Figure 23

SEM image of a feldspar grain with the quartz fraction of sample J0145

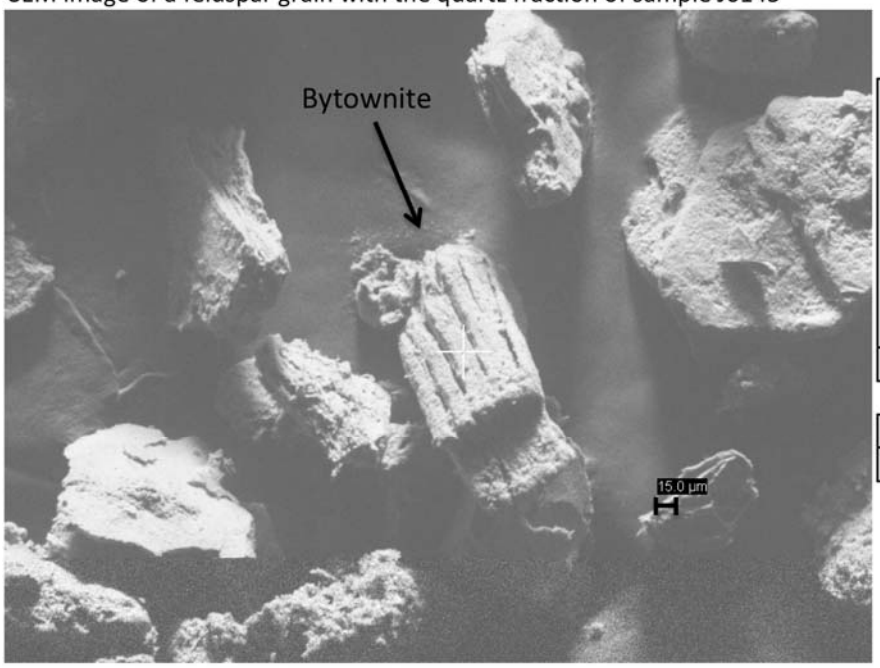

Element	Molar %
Na2o	10.01
MgO	33.99
AL2O3	31
SiO2	2.69
K2O	1.37
Ca0	17.72
TiO2	1.52
Feo	1.7
Total	100.00

Ca/(Na+Ca)	0.780
K/(K+Na)	0.120

Figure 23. Scanning Electron Microscope (SEM) image of a feldspar grain within the quartz fraction of sample J0145, suggesting that the laboratory density separations are not completely effective at separating out quartz and feldspar grains. This kind of contamination may contribute to the dim signals observed during quartz OSL measurements. Chemical analysis of this grain (marked with the +) indicates that this is a bytownite feldspar.

Figure 24

SEM image of a grain in the feldspar fraction of J0140

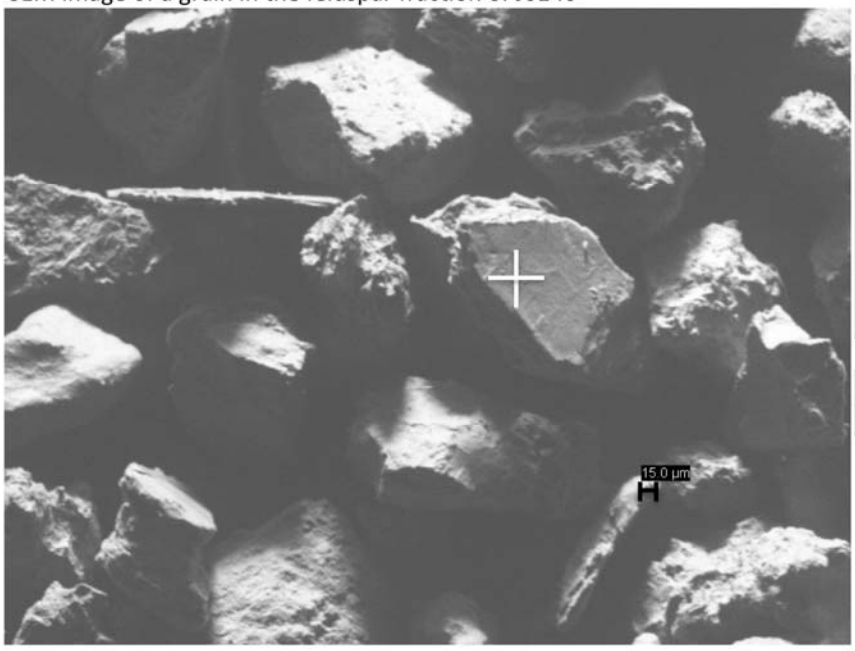

Element	Molar %
Na2o	2.78
MgO	4.75
AL2O3	9.52
SiO2	49.95
K2O	2.07
Ca0	1.44
Feo	29.49
Total	100.00

Ca/(Na+Ca)	0.509
K/(K+Na)	0.427

Figure 24. Scanning Electron Microscope (SEM) image of the feldspar fraction of sample J0140. In an attempt to quantify the species of feldspar present, chemical analysis of the surface of many grains (i.e. the grain marked with +) indicate a high iron content. This iron coating may contribute to the dim signals observed during feldspar IRSL measurements. Treating these grains with a quick (~10 min) etch in hydrofluoric acid (HF) resulted in a significant increase in grains that emitted a measurable luminescence signal during single-grain analysis. However, the D_e and age results were not

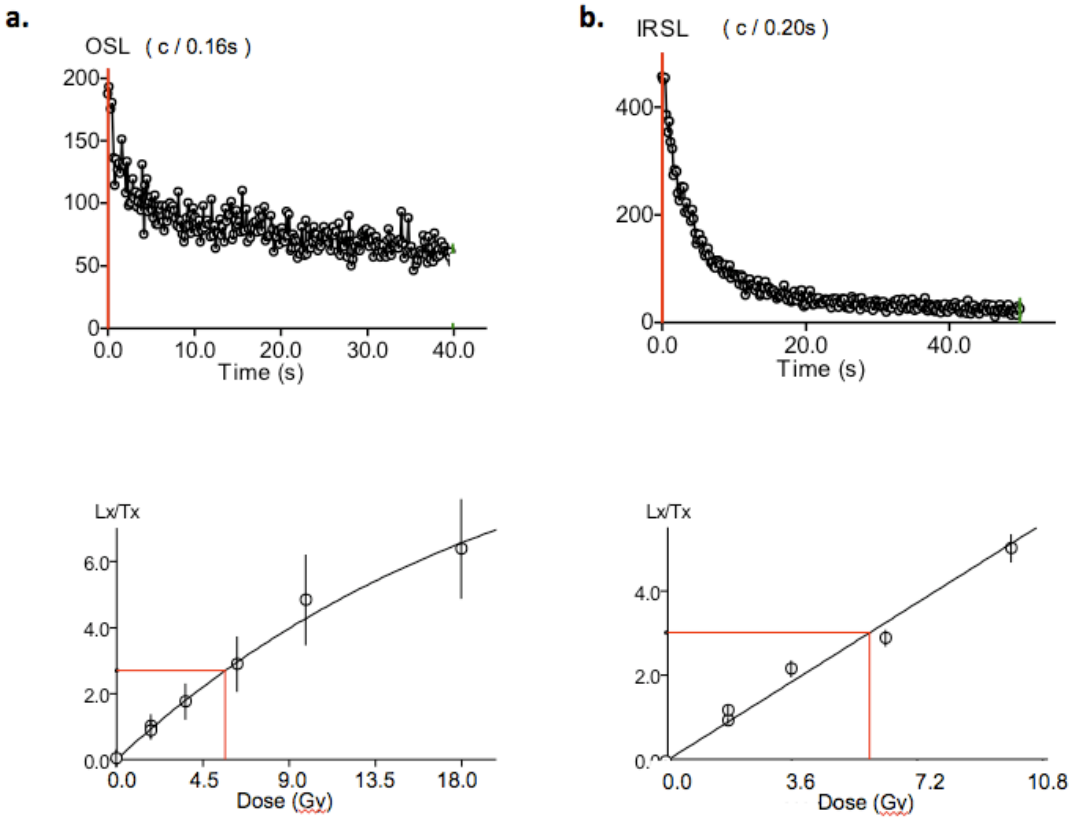

Figure 25. Decay curves (above) and growth curves (below) for (a.) quartz OSL and (b.) feldspar IRSL for CCW sample J0119. Quartz OSL measurements display low signal intensity and a high contribution from the slowly decaying components. Feldspar from this site also emits a dim signal.

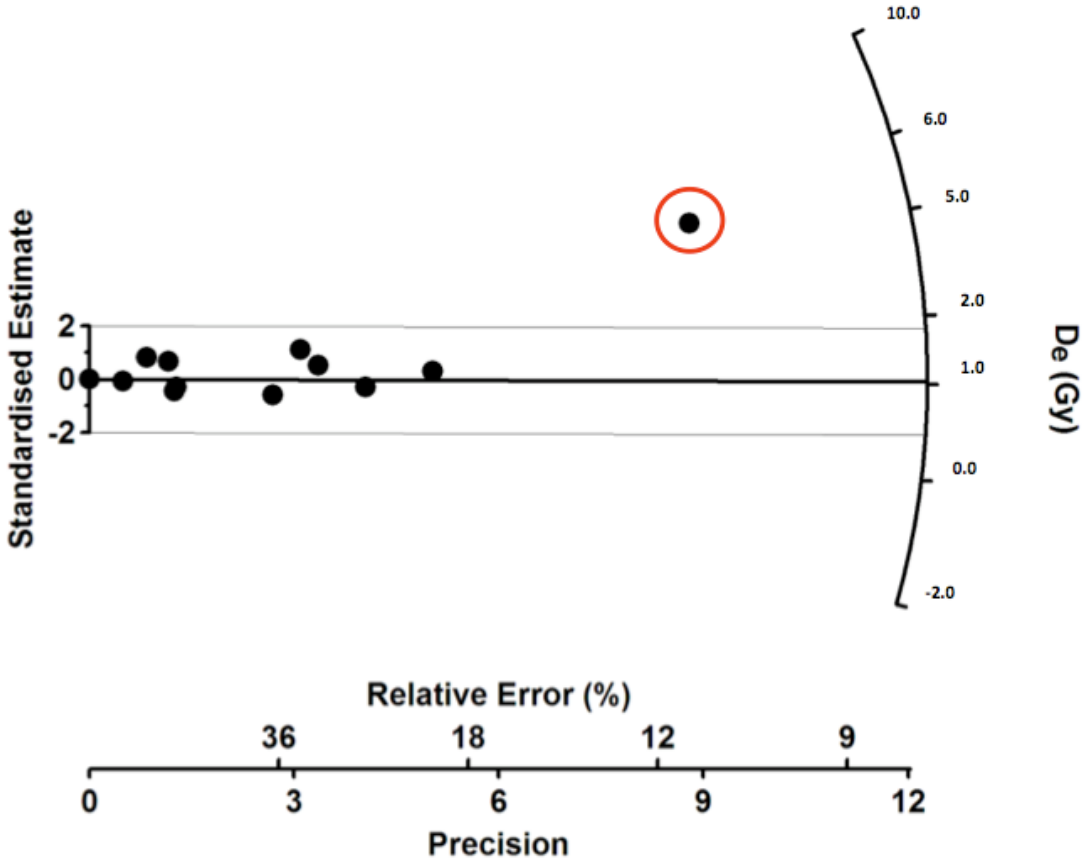

Figure 26. The synthetic super-aliquot approach was developed as a method for dealing with samples that suffer from incomplete bleaching (Bristow et al., 2010). This method discards unambiguously outlying high dose values (circled in red above), which are presumably not well bleached and contain a residual signal. The signals from the remaining aliquots are combined and used for D_e determination.

Figure 27

Christmas Canyon West OSL and IRSL age estimates.

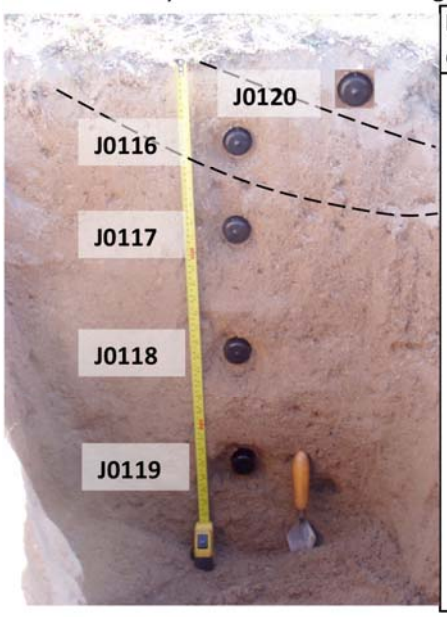

Laboratory code	Depth (cm)	Quartz OSL (years before 2012)	Feldspar IRSL (60°C) (years before 2012)
J0120	8	110 ± 70	110 ± 10
J0116	14	250 ± 60	250 ± 20
J0117	28	220 ± 200	480 ± 40
J0118	49	370 ± 70	890 ± 60
J0119	72	570 ± 110	1600 ± 80

Figure 27. Quartz OSL and feldspar IRSL age estimates at Christmas Canyon West. While initial quartz OSL age estimates appear in stratigraphic and in agreement with feldspar IRSL ages, comparison to feldspar IRSL age estimates using the post-IR IRSL protocol suggest that these initial underestimates are significantly underestimated.

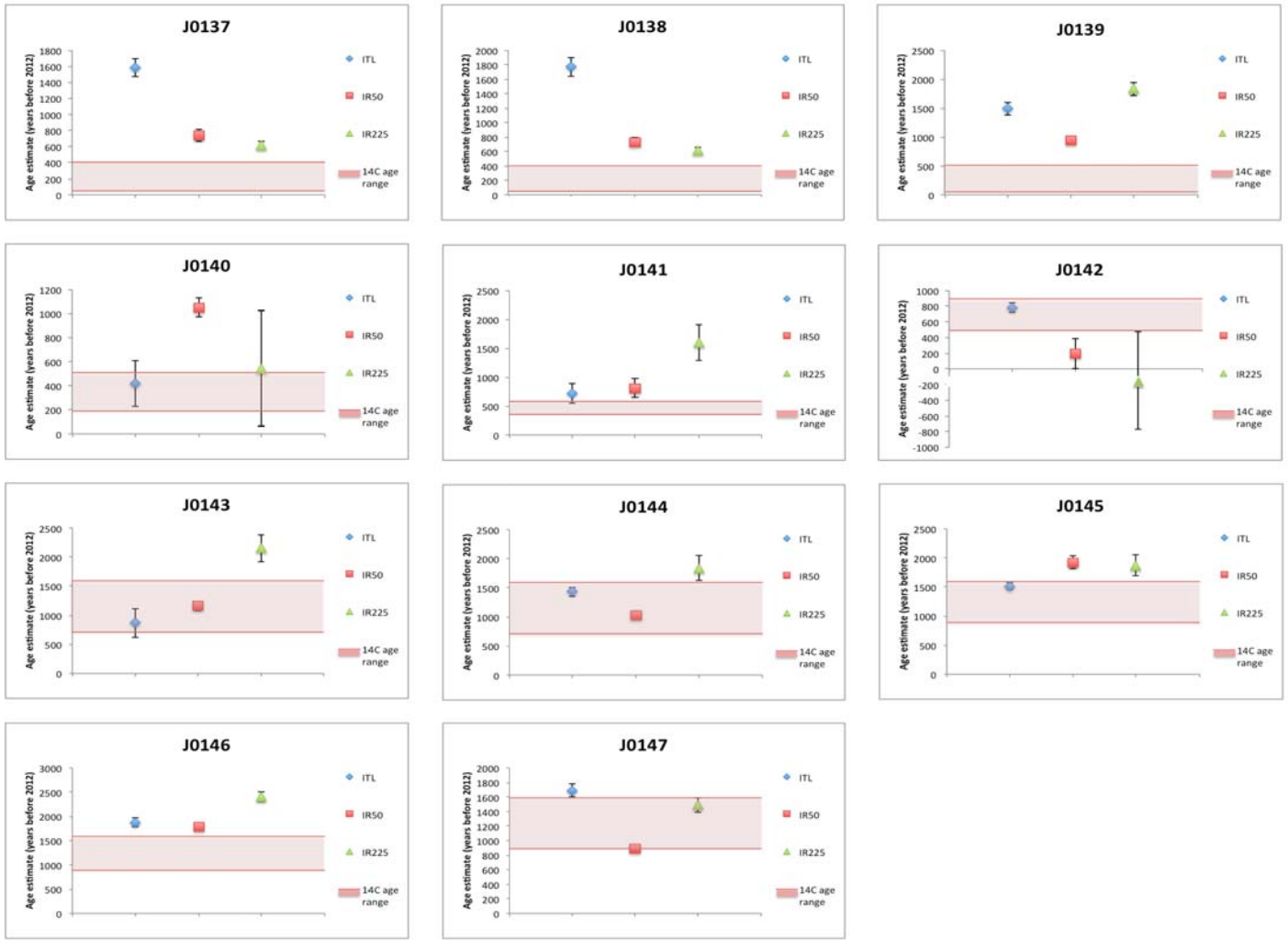

Figure 28. Comparison of the feldspar ITL, IR_{50}, and IR_{225} age estimates for EPP samples. Although uncorrected for fading, the ITL age estimates generally agree well with the radiocarbon age range from Dawson et al. (2003).

References Cited

Aitken, M.J., 1998. An introduction to optical dating; the dating of Quaternary sediments by the use of photon-stimulated luminescence. Oxford University Press, Oxford.

Auclair, M., Lamothe, M., Huot, S., 2003. Measurement of anomalous fading for feldspar IRSL using SAR. Radiation Measurements 37, 487-492.

Bailey, R.M., Smith, B.W., Rhodes, E.J., 1997. Partial bleaching and the decay form characteristics of quartz OSL. Radiation Measurments 27, 123-136.

Behr, W.M., Rood, D.H., Fletcher, K.E., Guzman, N., Finkel, R., Hanks, T.C., Hudnut, K.W., Kendrick, K.J., Platt, J.P., Sharp, W.D., Weldon, R.J., Yule, J.D., 2010. Uncertainties in slip-rate estimates for the Mission Creek strand of the southern San Andreas fault at Biskra Palms Oasis, southern California. Geological Society of America Bulletin 122, 1360-1377.

Bristow, C.S., Augustinus, P C., Wallis, I.C., Jol, H.M., Rhodes, E.J., 2010. Investigation of the age and migration of reversing dunes in Antartica using GPR and OSL, with implications for GPR on Mars. Earth and Planetary Science Letters 289, 30-42.

Buylaert, J.P., Murray, A.S., Thomsen, K.J., Jain, M., 2009. Testing the potential of an elevated temperature IRSL signal from K-feldspar. Radiation Measurements 44, 560-565.

Choi, J.H., Murray, A.S., Cheong, C.-S., Hong, D.G., Chang, H.W., 2006. Estimation of equivalent dose using quartz isothermal TL and SAR procedure. Quaternary Geochronology 1, 101-108.

Dawson, T.E., McGill, S.F., Rockwell, T.K., 2003. Irregular recurrence of paleoearthquakes along the central Garlock Fault near El Paso Peaks, California. Journal of Geophysical Research 108, No. B7, 2356, doi: 10. 1029/2001JB001744.

Dolan, J.F., Bowman, D.D., Sammis, C.G., 2007. Long-range and long-term fault interactions in Southern California. Geology 35, 855-858.

Duller, G.A.T., 2008. Luminescence Dating: Guidelines in Using Luminescence Dating in Archaeology. Swindon: English Heritage.

Fitzsimmons, K.E., Rhodes, E.J., Barrows, T.T., 2010. OSL dating of southeast Australian quartz: A preliminary assessment of luminescence characteristics and behavior. Quaternary Geochronology 5, 91-95.

Fletcher, K.E., Sharp., W.D., Kendrick, K.J.., Behr, W.M., Hudnut K.W., Hanks, T.C. 2010 230Th/U dating of a late Pleistocene alluvial fan along the southern San Andreas fault, Geological Society of America Bulletin 122, 1347-1359.

Frankel, K.L., Dolan, J.F., Owen, L.A., Ganev, P., Finkel, R.C., 2011. Spatial and temporal constancy of seismic strain release along an evolving segment of the Pacific-North America plate boundary. Earth and Planetary Science Letters 304, 565-576.

Huntley, D.J., Godfrey-Smith, D.I., Thewalt, M.L.W., 1985. Optical dating of sediments. Nature 313, 105-107.

Huntley, D.J., Lamothe, M., 2001. Ubiquity of anomalous fading in K-feldspars, and measurement and correction for it in optical dating. Canadian Journal of Earth Science 38, 1093–1106.

Huot, S., Buylaert, J.-P., Murray, A.S., 2006. Isothermal thermoluminescence signals from quartz. Radiation Measurements 41, 796-802.

Lawson, M.J., Roder, B.J., Stang, D.M., Rhodes, E.J., in press. OSL and IRSL characteristics of quartz and feldspar from southern California, USA. Radiation Measurements, in press.

Lian, O.B., Roberts, R.G., 2006. Dating the Quaternary: progress in luminescence dating of sediments. Quaternary Science Reviews 25, 2449-2468.

McGill, S.F., Rockwell, T.K., 1998. Ages of late Holocene earthquakes on the central Garlock Fault near El Paso Peaks, California. Journal of Geophysical Research 103, 7265-7279.

Murray, A. S., Wintle, A. G., 2000a. Luminescence dating of quartz using an improved single-aliquot regenerative-dose protocol. Radiation Measurements 32, 57-73.

Murray, A.S., Wintle, A.G., 2000b. Application of the single-aliquot regenerative-dose protocol to the 375°C quartz TL signal. Radiation Measurements 32, 579-583.

Murray, A. S., Wintle, A. G., 2003. The single aliquot regenerative dose protocol: potential for improvements in reliability. Radiation Measurements 37, 377-381.

Pietsch, T.J., Olley, J.M., Nanson, G.C., 2008. Fluvial transport as a natural luminescence sensitizer of quartz. Quaternary Geochronology 3, 365-376.

Preusser, F., Ramseyer, K., Schluchter, C., 2006. Characterisation of low OSL intensity quartz from the New Zealand Alps. Radiation Measurements 41, 871-877.

Rendell, H.M., Lancaster, N., Tchakerian, V.P., 1994. Luminescence dating of late Quaternary deposits at Dale Lake and Cronese Mountains, Mojave Desert, California. Quaternary Geochronology 13, 417-422.

Rhodes, E.J., 2007. Quartz single grain OSL sensitivity distributions: implications for multiple grain single aliquot dating. Geochronometria 26, 19–29.

Rhodes, E.J., Fanning, P.C., Holdaway, S.J., 2010. Developments in optically stimulated luminescence age control for geoarcheological sediments and hearths in western New South Wales, Australia. Quaternary Geochronology 5, 348-352.

Rhodes, E. J., 2011. Optically stimulated luminescence dating of sediments over the past 200,000 years. Annual Review of Earth and Planetary Sciences 39, 461-488.

Steffen, D., Preusser, F., Schlunegger, F., 2009. OSL quartz age underestimation due to unstable signal components. Quaternary Geochronology 4, 353-362.

Spooner, N.A., 1994. On the optical dating signal from quartz. Radiation measurements, 23, 593-600.

Thomsen, K.J., Murray, A.S., Jain, M., Botter-Jensen, L., 2008. Laboratory fading rates of various luminescence signals from feldspar-rich sediment extracts. Radiation Measurements 43, 1474-1486.

Van der Woerd, J., Klinger, Y., Sieh, K., Tapponnier, P., Ryerson, F.J., Meriaux, A-S., 2006. Long-term slip rate of the southern San Andreas fault from 10Be-26Al surface exposure dating of an offset alluvial fan. Journal of Geophysical Research 111(B4), 17 pp.

Wallinga, J., Bos, A.J.J., Dorenbos, P., Murray, A.S., Schoker, J., 2007. A test case for anomalous fading correction in IRSL dating. Quaternary Geochronology 2, 216-221.

Wintle, A., 1973. Anomalous fading of thermoluminescence in mineral samples. Nature, 245(5421), 143-144.

Wintle, A.G., Murray, A.S., 2006. A review of quartz optically stimulated luminescence characteristics and their relevance in single-aliquot regeneration dating protocols. Radiation Measurements 41, 369-391.